ISSN 8755-6839

SCIENCE OF **TSUNAMI HAZARDS**

Journal of Tsunami Society International

Volume 33 **Number 2** **2014**

WWW.TSUNAMISOCIETY.ORG

TSUNAMI SOCIETY INTERNATIONAL, 1741 Ala Moana Blvd. #70, Honolulu, HI 96815, USA.

SCIENCE OF TSUNAMI HAZARDS is a CERTIFIED OPEN ACCESS Journal included in the prestigious international academic journal database DOAJ, maintained by the University of Lund in Sweden with the support of the European Union. SCIENCE OF TSUNAMI HAZARDS is also preserved, archived and disseminated by the National Library, The Hague, NETHERLANDS, the Library of Congress, Washington D.C., USA, the Electronic Library of Los Alamos, National Laboratory, New Mexico, USA, the EBSCO Publishing databases and ELSEVIER Publishing in Amsterdam. The vast dissemination gives the journal additional global exposure and readership in 90% of the academic institutions worldwide, including nation-wide access to databases in more than 70 countries.

OBJECTIVE: Tsunami Society International publishes this interdisciplinary journal to increase and disseminate knowledge about tsunamis and their hazards.

DISCLAIMER: Although the articles in SCIENCE OF TSUNAMI HAZARDS have been technically reviewed by peers, Tsunami Society International is not responsible for the veracity of any statement, opinion or consequences.

Submit manuscripts of research papers, notes or letters to the Editor. If a research paper is accepted for publication the author(s) must submit a scan-ready manuscript, a Doc, TeX or a PDF file in the journal format. Issues of the journal are published electronically in PDF format. There is a minimal publication fee for authors who are members of Tsunami Society International for three years and slightly higher for non-members. Tsunami Society International members are notified by e-mail when a new issue is available. Permission to use figures, tables and brief excerpts from this journal in scientific and educational works is granted provided that the source is acknowledged.

Recent and all past journal issues are available at: http://www.TsunamiSociety.org CD-ROMs of past volumes may be purchased by contacting Tsunami Society International at postmaster@tsunamisociety.org Issues of the journal from 1982 thru 2005 are also available in PDF format at the U.S. Los Alamos National Laboratory Library http://epubs.lanl.gov/tsunami/

ISSN 8755-6839

SCIENCE OF **TSUNAMI HAZARDS**

Journal of Tsunami Society International

Volume 33 **Number 2** **2014**

REMOTE: RECONNAISSANCE AND MONITORING OF TSUNAMI EVENTS

Frank C. Lin[1*], Kingkarn Sookhanaphibarn[1], Virulh Sa-yakanit[2], George Pararas-Carayannis[3]

[1]Multimedia Intelligent Technology Laboratory
School of Science and Technology, Bangkok University
Rama 4 Rd, Khlong Toei, Bangkok 10110, Thailand.

[2]Center of Excellence in Forum for Theoretical Science
Department of Physics, Faculty of Science, Chulalongkorn University
Bangkok 10330, Thailand

[3]Tsunami Society International, Honolulu, Hawaii 96815, USA

ABSTRACT

The present study describes a prototype we built and named REMOTE for detecting and monitoring in real time tsunami events, based on changes in infrared radiation emitted from the sea when up thrust crustal movements from a major or a great tsunamigenic earthquake disturb the ocean floor and change the thermal properties of the water column in the source region. Specifically, we describe the hardware and software components of this system and present its performance results from recent tsunamis. Declouding of satellite images is often required and this is accomplished by the application of wavelet analysis. Also, in the present study we address the problem of signal delay due to the satellite scanning cycle and discuss possible solutions. Finally, we enumerate the relative benefits of our system. Our proposed system is available to all the countries with access to a geostationary weather satellite.

Keywords: *Tsunami Warning, Infrared Space, REMOTE, Tsunami Signal, Weather Satellite*

**Corresponding author. Email:linbfrank@gmail.com. Tel/Fax: +662 612 4705.*

1. INTRODUCTION

Tsunami(s) are a series of destructive ocean waves usually generated by major or great earthquakes along zones of tectonic subduction where tectonic plates collide. By far, the most destructive tsunamis are caused by large, shallow earthquakes with epicenter or fault line near or on the ocean floor. Displacements of the earth's crust along a rupture resulting from such large earthquakes, lift up the water and generate tsunami waves that can travel across the ocean spreading destruction along their path. Similar displacements of the ocean floor by volcanic eruptions, submarine avalanches, submarine landslides, rock falls and even asteroids can also generate tsunamis. In deep water, tsunamis are characterized by relatively low amplitude, usually less than one meter, but their wavelengths can be hundreds of kilometers long. Thus a tsunami cannot be felt aboard ships in deep water.

In order to mitigate destruction and loss of lives once a tsunami is generated, it is important to have an effective warning system to inform the population in vulnerable coastal areas to evacuate to designated safe zones at higher elevations. The purpose and rationale of the present paper is to assist in such disaster mitigation efforts by providing in real time an alternative and inexpensive method for the early detection and monitoring of a potentially destructive tsunami.

Present methods of detecting and measuring tsunamis in near real time, include coastal tide gauges as well as bottom gauges, such as the "Deep-Ocean Assessment and Reporting of Tsunami" (DART), which essentially measure aquatic pressure changes when a tsunami wave reaches them. The DART system functions as follows: Pressure sensors are placed on the ocean bottom near known earthquake zones. Each deep-water station is equipped with an acoustic modem transducer, which encodes the data into sound waves. An anchored, communications buoy on the ocean surface processes the information and sends it by radio waves to a weather satellite (GOES). Based on such transmitted data, computers at ground stations provide estimates of the tsunami's source region as well as estimates of its wave speed and arrival times at different coastal areas. However, hydrostatic pressure changes recorded by a DART gauge may not be necessarily triggered by a tsunami and, consequently, there are high rates of false alarms. According to Gonzalez [1999] and others, approximately 75% of all warnings issued between 1948 and 1999 were false. Of course, during the early time period, there were no DART stations and in the 90's there were only a few installed and their technology was still under development. The present performance of DART stations has improved since 1999. In this present paper we present a direct, novel and more economical method than DART, which promises, in conjunction with the earthquake detection, to give nearly unequivocal results on detection of tsunami generation.

The main question addressed by the present study is the following: If an undersea earthquake has been detected, by the USGS, the Japan Meteorological Agency or another earthquake monitoring organization, how can it be conclusively determined if a tsunami was indeed generated by this

earthquake? The present study answers this question positively and illustrates how with proper methodology and processing of data from an infrared geostationary satellite, the generation of a tsunami can be detected and monitored. However, at present, we do not account for the propagation of the tsunami, only for its detection and approximate dimensions of the generating source region.

In previous communications [Lin *et al.*, 2010; Lin and Sookhanaphibarn, 2011; Lin *et al.*, 2011; Lin *et al.*, 2012] we publicized our discovery that when tsunamis are generated by a large earthquake, there is infrared radiation of circa 11μm which can be detected by a geostationary satellite. In this paper we present a brief overview of our findings. In addition, we add some new results, which confirm our previous findings, as well as some exceptions (the 2010, Bio-Bio event in Chile and the 2011 Ofunato, Japan event of 2011), for which reasonable justifications are given. Furthermore, we discuss in greater detail the problem of defining tsunami magnitude, which cannot be associated with phase space variables and the application of wavelet analysis to de-clouding methodology, using the great 2004 North Sumatra tsunami as an example. Additionally, but to a limited extent, we compare the advantages of our proposed system of tsunami detection vis-à-vis with that of DART. Finally, we describe in detail both the hardware and software system of our REMOTE system so that it can be appraised, analyzed or replicated, in the belief that it will – when universally implemented - mitigate future loss of life and property from the tsunami hazard.

2. METHOD AND DATA

2.1 Hardware Implementation

A PC-based data receiving and processing system is used to implement the REMOTE tsunami early detection system. The system is designed to receive high frequency satellite signals at approximately 1687 MHz, deploying a parabolic antenna, as shown in Figure 1, of 3m diameter. The gain is 33 dB. A sample of the real-time satellite image is shown in Figure 2 below.

Fig. 1: Disk antenna.

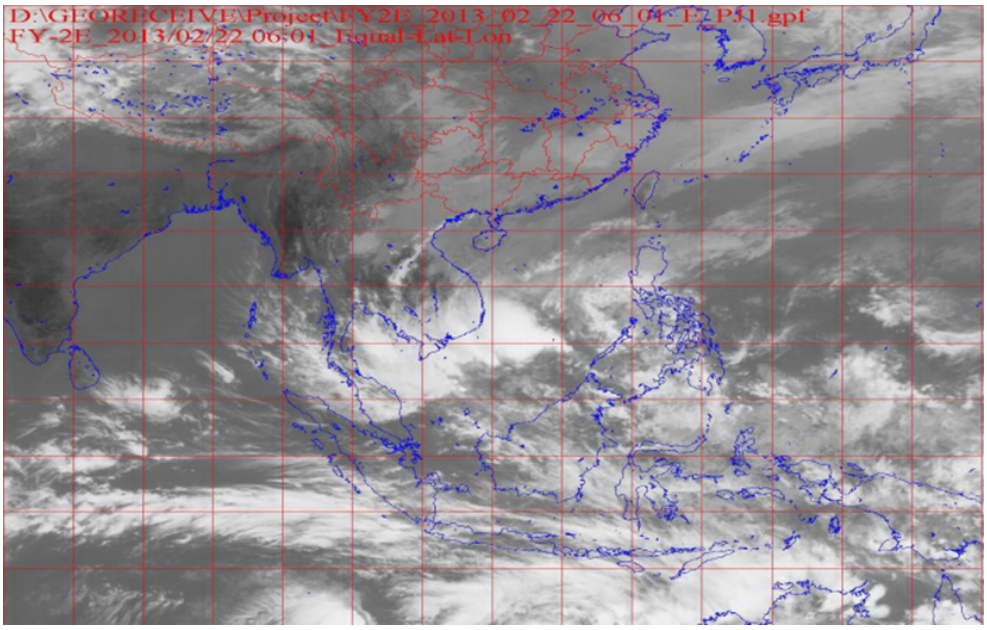

Fig. 2: Real-time satellite image from FY-2E.

The signal from the antenna is fed into a low noise block down-converter (LNA) which is a combination of low-noise amplifier, frequency mixer, local oscillator and IF (Inter-mediate Frequency) amplifier. The LNA switches the signal to an intermediate frequency of 137.5 MHz, which can then be transferred indoors. A receiver in turn converts this to a second intermediate frequency signal of 10.7 MHz. The bandwidth of the receiver is 1.5 MHz and the gain is greater than or equal to 70 dB. After filtering, amplifying and demodulation, the fundamental band signal of 660 kbps is generated. This band signal is further processed by a bit synchronizer for clock extraction and code conversion, and a frame synchronizer for frame synchronous signal detection, channel separation and data format conversion. Finally, these data are input into the 2 PCs (Front end and back end) via a PCI ingestor card, which serves as an interface device, for software processing. A flow diagram for the hardware portion of our system is shown in Figure 3.

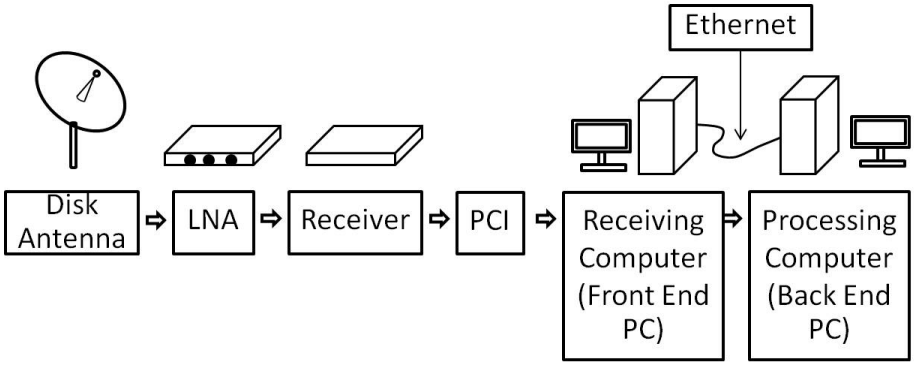

Fig. 3: Flowchart of the hardware portion of REMOTE system.

The front end PC is in charge of data ingesting, viewing, map projection and ftp transfer of the geostationary satellite data (Digital Video Broadcast). The back end PC performs the functions of displaying the image and creating animations and applications. The viewing part of the DVBS displays the channel image in RGB and the scan line information at the title bar. Also, it draws the latitude and longitude grid, political boundaries and geographical features on the image. The IR channel data of each scan line has 2291 scan points, only half of which are displayed on the screen at one time. Five different projection types can be selected. The observation range of the geostationary satellite extends 60 degrees from the Sub-Satellite Point (SSP). The resolution of the IR channel is 5 km. This resolution is adequate for the detection of tsunamis, since the extent of the tsunami signal at the ocean surface is usually 10 to 20 km (two pixels or more). A smaller size of projection image is possible.

The back end PC is mainly an image processing and sub-function producing unit. It has the capability to perform many functions, such as detecting edges, setting palettes, adjusting colors, overlaying maps and contours, etc. It can also add grids, maps, communication lines, and other GIS information. Generated sub-functions include Cloud Cluster Area, Typhoon Location, Precipitation Estimation, Sea Surface Temperature, Outgoing Long Wave Radiation, etc. For our prototype we have directly installed our software in the back end PC. Other options, such as using an Ethernet connection, are possible.

2.2 Software Implementation

Once the satellite image is made available, it is necessary to analyze the image to ascertain whether a tsunami has occurred and, if affirmative, a tsunami warning must be sent to potentially vulnerable areas. A prompt and unambiguous warning sent to the relevant Civil Defense Authorities can save many lives. We describe below the software that we have developed for this purpose. This software can be used in real time in conjunction with the hardware described above, or it can be used independently to analyze historical events. The fundamental physics involved is our observation - as reported in several publications previously - that a tsunami generates an infrared radiation of circa 11 μm (900 cm^{-1}), which can be detected by a geostationary satellite in the infrared domain.

We have implemented the software in MATLAB. The flow diagram for this process is shown in Figure 4 [Lin *et al.*, 2013].

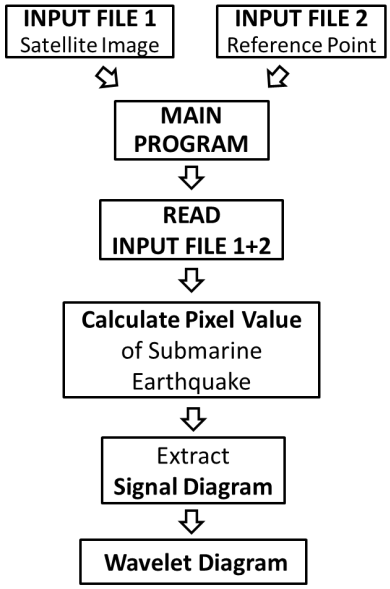

Fig. 4: Processing flowchart of REMOTE system.

In the historical mode, the software reads in the satellite image and two arbitrary reference points whose geodetic positions are known. It calculates the pixel value of the position of submarine earthquake using an interpolation procedure. Then it extracts the Signal Diagram from the satellite image, from which the Wavelet Diagram follows. In the real time mode, this process is continuous and automatic. If a tsunami signal is recognized, a warning is immediately issued. The delay from the time of the submarine earthquake and the tsunami warning is typically minutes.

The following program lines illustrate how the Signal Diagram is extracted from the satellite image:

Algorithm 1:
begin
load(*JPGfilename*, *Ytsunami* , *Xtsunami*)
imageDat =imread(*JPGfilename*)
rowDat = imageDat(*Ytsunami* ; :)
columnDat = imageDat(:; *Xtsunami*)
return(*rowDat, columnDat*)
end

Here, *rowDat* is the latitudinal Signal Diagram and *columnDat* the longitudinal Signal Diagram. *Y* ; *Xtsunami* are the coordinates of the earthquake epicenter, and *JPEGfilename* refers to the satellite image.

The Signal Diagrams are then plotted in *Algorithm 2*:

Algorithm 2:
begin
x=1:length(*rowDat*)
y=1:length(*columnDat*)
plot(x, *rowDat*, 'grid on') and title('East-West Signal Diagram')
plot(y, *columnDat*, 'grid on') and title('North-South Signal Diagram')
Finally, the Wavelet Diagram is constructed.
end

The flow chart of the integrated REMOTE (Reconnaissance and Monitoring of Tsunami Events) system is shown in Figure 5.

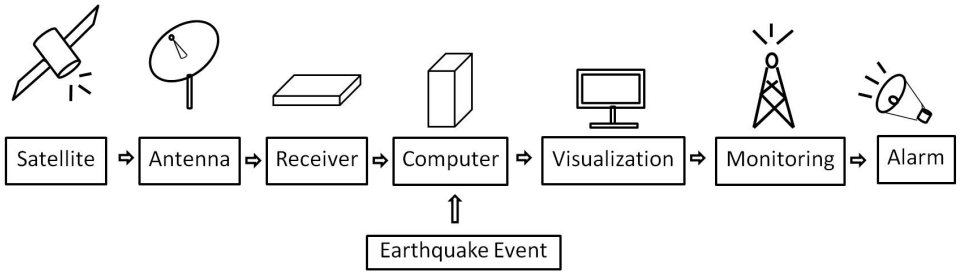

Fig. 5: REMOTE (Reconnaissance and Monitoring of Tsunami Events) flowchart.

3. RESULTS

In the following section we compile a catalogue of recent tsunamis and apply our methodology to evaluate them in order to identify as well as to understand the source origin of tsunamis in infrared space. Our study complements the knowledge gained from the DART system and in particular empowers us to devise a new, satellite-based, early warning system, which responds instantaneously when a tsunami is generated. Specifically, we show the following: 1) A tsunami emits infrared radiation at circa 11 μm; 2) This radiation, called the tsunami signal, can be detected by a geostationary satellite in the infrared domain; 3) This radiation is capable of penetrating extensive cloud cover, which can be demonstrated using the denoising properties of wavelet analysis; 4) The half-life of the tsunami signal is about half an hour and its spatial extent is about 10-20 km; 5) The time delay between the submarine earthquake and the broadcasting of the tsunami by the satellite is typically within minutes; 6) There are no false positives or false negatives (with one exception); and 7) The vector representation of tsunamis in phase space and in infrared space can be mapped into each other by a linear transformation [Lin and Sookhanaphibarn, 2011].

Table 1 shows the Earthquake Magnitude and the tsunami signal, S (see Section IV).

Table 1: Recent Tsunami Events.

Location	**Lat.**	**Long.**	**Date and Time (UTC)** (yy-mm-dd hh:mm:ss)	***Me***	***S* pixels**
Sumatra	3.3	95.8	2004-12-26 00:58:53	9.0	417
Tohoku	38.3	142.4	2011-03-11 05:46:24	9.0	255
Chile	35.8	72.7	2010-02-27 06:34:00	8.8	170
N.Sumatra	2.31	93.0	2012-04-11 08:38:37	8.6	203
Philippines	10.8	106.8	2012-08-31 12:47:34	7.6	210

3.1 The 2004 Sumatra-Andaman (Banda Aceh) Tsunamigenic Earthquake

On Dec. 26, 2004 a gigantic tsunami in the Indian Ocean was triggered by the subduction of the Indian plate beneath the Burma plate near the Indonesian city of Banda Aceh. The India Plate meets the Burma Plate (which is a portion of the Eurasian Plate) at the Sunda Trench. At this point the India Plate subducts beneath the Burma Plate, which includes the Nicobar Islands, the Andaman Islands and northern Sumatra. According to the USGS, the northern section of the Sunda megathrust, which had been established as a seismic gap, ruptured - the rupture having a total length of 1,300 km. An inspection of the thermal profile of the Indian Ocean shows that the water temperature decreases from around 25 degrees at the surface to about 5 degrees one kilometer below and eventually attaining 4 degrees ten kilometers below. At the onset of tsunami event generation, the sudden crustal movements of the ocean floor caused by the earthquake lift cold water up to the surface. The tsunami burst is therefore characterized by a sudden temperature gradient, which in turn triggers the emission of a thermal tsunami signal. Meteorological satellites such as the Chinese FY-2C, which is geostationary on the earth's equator at Longitude $105°$ and recording wavelengths ranging between 3.5 and 12.5 μm, are able to detect this change in infrared domain. For this particular Chinese satellite, the temperature resolution is 0.5 K and the space resolution is 5 km.

In Figure 6 we show the tsunami signals, i.e. the infrared radiation detected by the FY-2C (also called the pixel brightness when referring to the satellite image), along the latitude of Banda Aceh, at 7 A.M. and 8 A.M. local time, respectively. Because of the temperature gradient of the thermo cline, we expect that the tsunami signal will show up in the latter figure but not in the former.

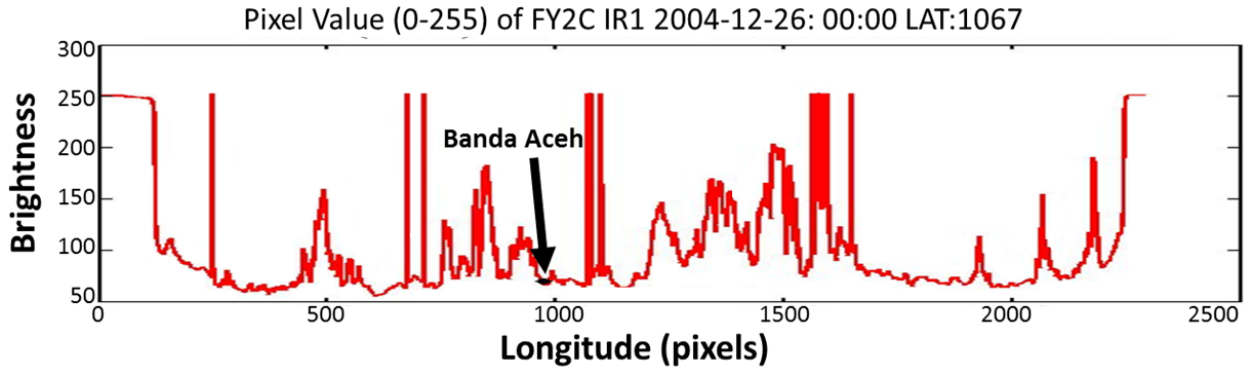

(a)

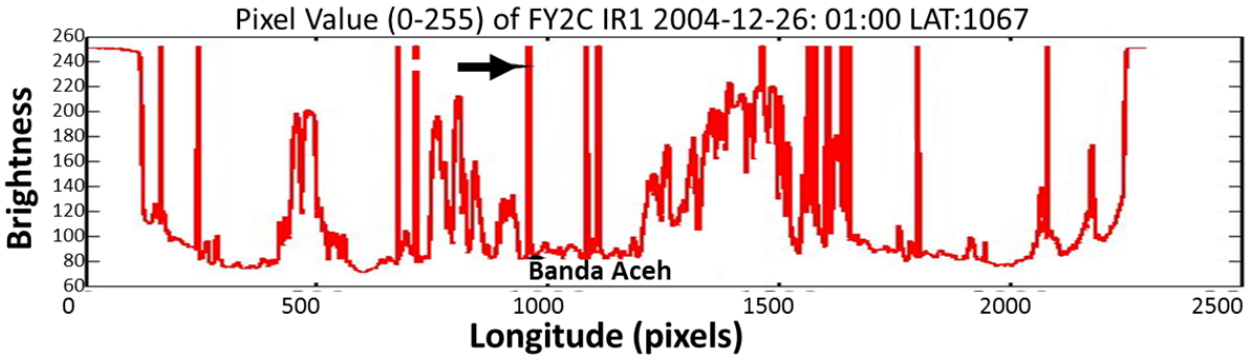

(b)

Fig. 6: Signal along Latitude 1067 pixels (latitude of Banda Aceh) at a) 7.00 A.M. and b) 8.00 A.M.

Comparison of Figure 6a and Figure 6b shows that at the location of Banda Aceh, a very strong signal appears at 8 A.M. local time (pointed to by an arrow in Figure 6b), which is absent at 7 A.M. (Figure 6a). Given the time and the location of the spike, there is no doubt that this is the anticipated tsunami signal. We emphasize again that the time and the location define a unique point in four-dimensional space-time with x, y, z, t coordinates (Minkowski space). There is only one spike which satisfies these criteria. In the Signal Diagrams and the Wavelet Diagrams, the tsunami signal is located at the longitude of the submarine earthquake origin. ***All other spikes cannot be attributed to the tsunami signal, since they originate at longitudes where no submarine earthquakes occurred at this point of space-time.***

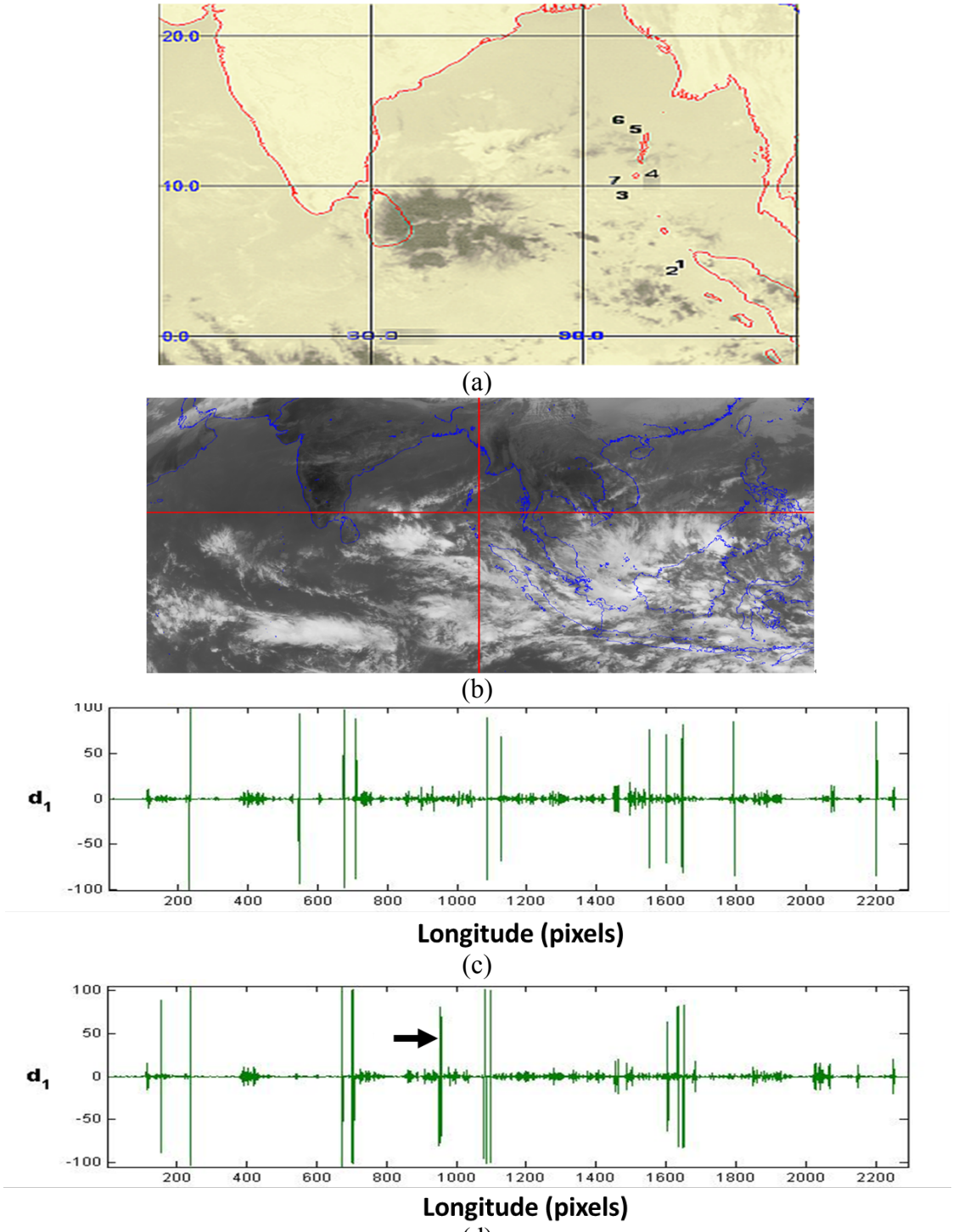

Fig. 7: Aftershocks in Sumatra-Andaman (Banda Aceh) region: a) Location of aftershocks; b) Satellite photo of epicenter for ANDAMAN-Location 2 at 08:00 A.M.; c) Detailed decomposition of the aftershock signal at 09:00 A.M. and d) at 10:00 A.M., respectively.

Figure 7a, shows the locations of the main shock (Position 1) and of some of the subsequent aftershocks (Positions 2 to 7). A satellite image of the Indian Ocean is shown in Figure 7b. It is noteworthy that except for positions 5 and 6 surrounding the Andaman Islands, a tsunami signal is sighted in all other cases, indicating that the colder water from the bottom of the ocean reached the surface and, consequently and unambiguously, a tsunami had been generated - although no flooding at nearby land areas has yet been recorded. In particular, a strong aftershock at location 2 occurred an hour later at the same latitude. Figures 7c and 7d show the Wavelet Diagrams of this event at 9 A.M. and 10 A.M. respectively. In Figure 7c, (9 A.M.) no tsunami signal is seen at the earthquake epicenter, whereas a tsunami signal is distinctly visible in Figure 7d (10 A.M.), as pointed by an arrow. Wavelet analysis is particularly appropriate since it is capable of denoising the satellite images without appreciable degradation.

3.2 The 2011 Tohoku Tsunamigenic Earthquake

On Friday, March 11, 2011 at 05:46:24 UTC (02:46:24 P.M., local time) a great earthquake with a moment magnitude of 9.0 occurred at a depth of 30 km, about 129 km east of Sendai Island of Honshu in Japan. The quake epicenter was at 38.297°N and 142.372°E near the zone of subduction where the Pacific plate moves westward, descending beneath Japan. As a result of this earthquake the coast of northeast Japan moved eastward by about 4 meters and the coastline generally subsided by up to 1.1 meter. The great Tohoku-Oki earthquake - as it was named - generated a very destructive and anomalously high tsunami with a distinct source mechanism [Pararas-Carayannis, 2013]. According to the USGS, the total slip of the quake was approximately 300 km long and 150 km wide. At least 15,703 people lost their lives and at least 332,395 buildings were destroyed or damaged by the combined impact of the earthquake and tsunami along the entire east coast of the Island of Honshu. The maximum tsunami run-up height was 37.88 m at Miyako, very similar to that caused by the 1896 tsunami generated by the Great Tohoku earthquake [Pararas-Carayannis, 2013]. The economic loss in Japan from the 2011 disaster was estimated to be more than 300 billion in U.S. dollars.

In the present study we have systematically investigated the main shock of this event as well as the foreshock and four major aftershocks with the help of the methodology that we have developed and described. The results are summarized in Table 2 [Lin *et al.*, 2011; Lin *et al.*, 2012]. The quantity S in Table 2 represents the tsunami magnitude (Section IV).

Table 2: Tohoku Earthquake - Foreshock and major aftershocks.

Event	Me	Date and Time (UTC) (yy-mm-dd hh:mm)	Lat.	Long.	S pixels	Mt
Main-shock	9.0	2011-03-11 05:46	38.30N	142.37E	255	7.99
Foreshock	7.2	2011-03-09 02:45	38.42N	142.64E	197	7.62
Aftershock-1	7.1	2011-04-07 14:32	38.25N	141.64E	161	7.33
Aftershock-2	6.6	2011-04-11 08:16	37.01N	140.48E	none	N/A
Aftershock-3	7.9	2011-03-11 06:15	36.27N	141.14E	255	7.99
Aftershock-4	7.7	2011-03-11 06:25	38.05N	144.59E	none	N/A

The main conclusions of the present investigation about this event are as follows:

(1) The foreshock on 2011-3-9 had a moment magnitude of 7.62. In the wavelet diagram in Figure 8, a strong tsunami signal is shown as pointed to by an arrow. This foreshadowed the main shock that followed on 2011-3-11. It might have been possible to predict the nucleation and subsequent occurrence of the main shock by using a non-linear forecasting technique such as the Back-propagation Neural Network [Lin and Mohamed, 1999; Lin *et al.*, 2002].

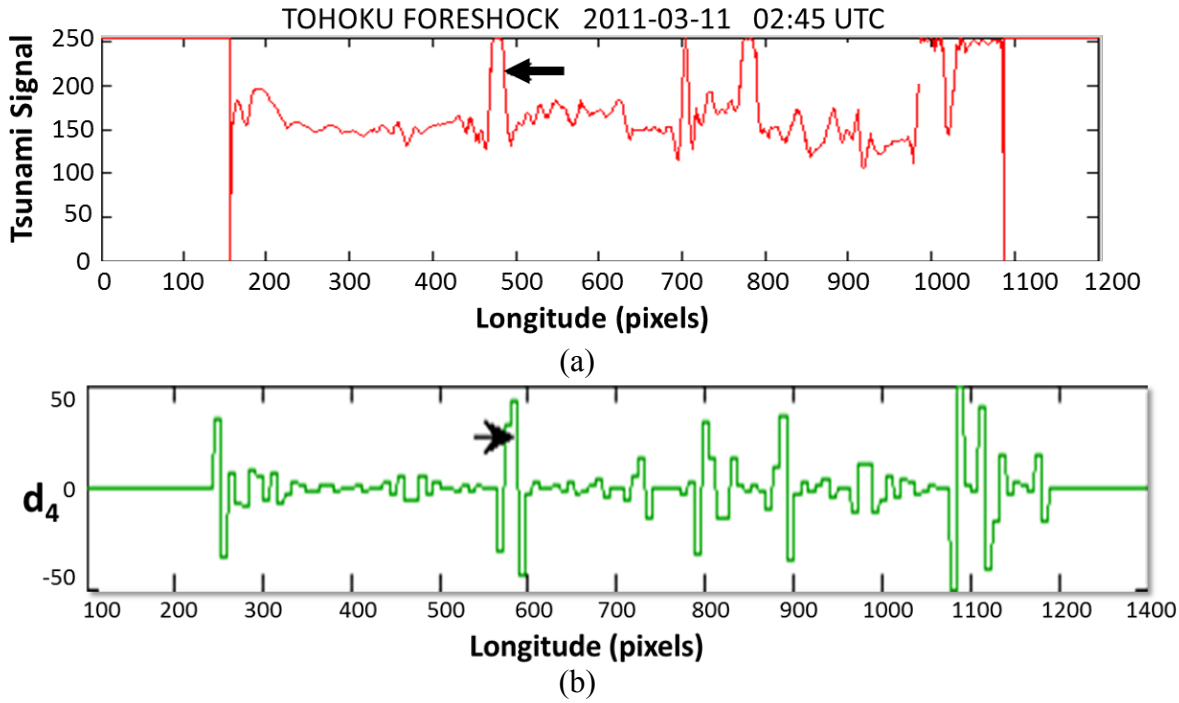

Fig. 8: Tohoku Foreshock event of 2011-3-9: a) Signal Diagram; b) Wavelet Diagram.

(2) The results obtained by remote sensing correlate with and are synchronized with the DART data. In Figure 9, we show the Wavelet diagrams for the main shock, aftershock-3 and aftershock-4, all of which occurred on the same day. Also shown are the readings from DART buoy #21418, which was closest to the tsunami source region. It is seen from Figure 9 that both the main shock and aftershock-3 were registered by the DART buoy, as indicated by the arrows. However, the satellite data did not show a tsunami signal for aftershock-4 and similarly, the DART buoy did not register an earthquake for aftershock-4. There was no spike for afterschock-4.

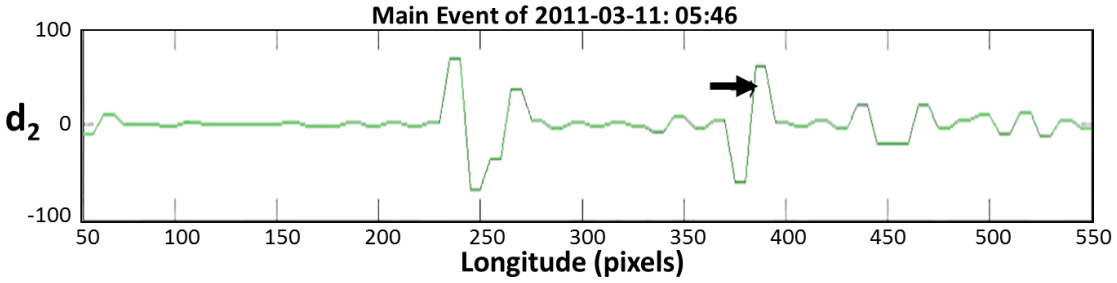

(a)

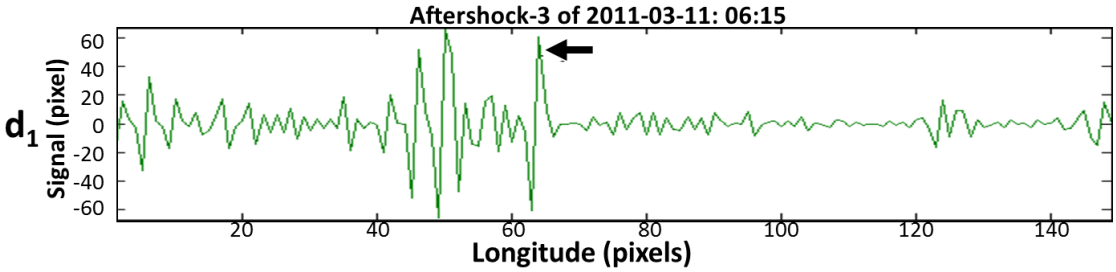

(b)

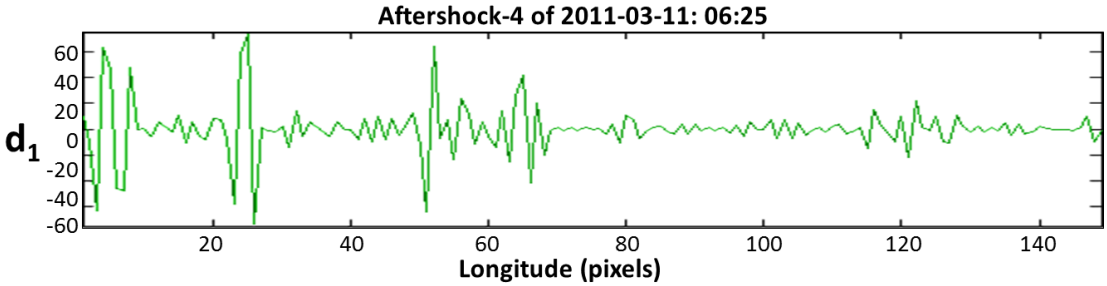

(c)

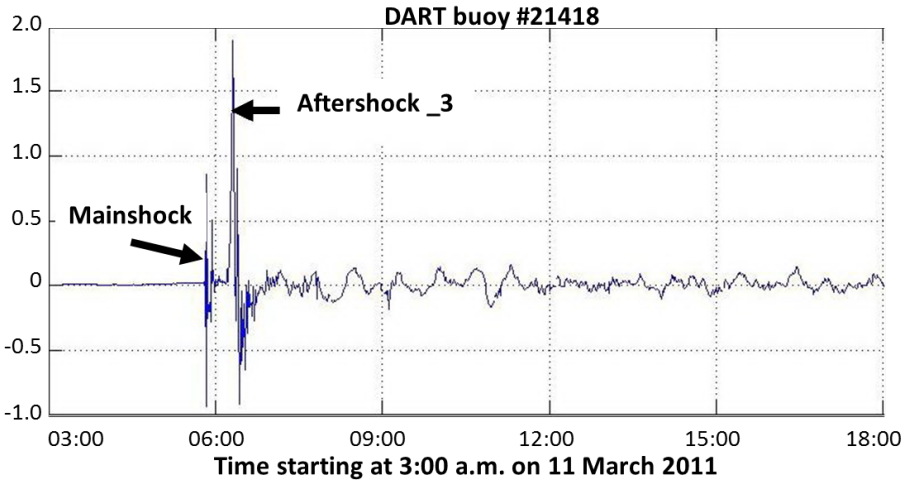

(d)

Fig. 9: Satellite data compared with DART data.

Within one hour after the earthquake the tsunami reached the Fukushima Daiichi Nuclear Power Plant, which consists of six boiling water reactors. A maximum 15-meter high tsunami wave easily overflowed the plant's 6-meter protective seawall. The nuclear facility was not prepared for such an emergency and a partial meltdown occurred at reactors #1 and #3. Subsequently, a fire and an explosion at reactor #4 released radioactivity directly into the atmosphere.

3.3 The 2010 Chile BIO-BIO Tsunamigenic Earthquake

On February 27, 2010 an 8.8 magnitude earthquake occurred at 06:34 UTC. Its epicenter was at 35.8°S and 72.7°W, approximately 115 km north of Concepciòn, Chile. The earthquake was triggered by a thrust-faulting focal mechanism occurring at the high rate of 6.8 centimeters per year along an active, oblique subduction zone where the Nazca tectonic plate thrusts below South America. This was the 6th most powerful earthquake in recorded history and the largest in the region since the extremely destructive May 22, 1960 magnitude 9.5 earthquake near Valdivia. In Valparaiso, a tsunami wave of 1.29 m was reported. In spite of the severity of the earthquake, only 525 people lost their lives due to the combined impact of the earthquake and tsunami.

Using GPS data, it was determined that Concepciòn moved at least 3 meters to the west. This movement may have had consequences on the hydrodynamics of the rising cool water following the earthquake. A satellite image taken on 2010-02-27 at 06:39 UTC by GOES-12 is shown in Figure 10a. The blue lines are latitudes and longitudes and the red line delineates the coast of Chile. A flag (white space with x, y pixel values) designates the epicenter of the earthquake. Figure 10b shows the latitudinal (a slice of the satellite image showing the distribution of the pixel brightness along the latitude of the epicenter) Signal Diagram. The spikes pointing downwards are the longitudinal lines.

According to the USGS the epicenter of the earthquake was about 3 km off the coast of Pelluhue commune in the Maule Region. Since the resolution of the satellite image is approximately 5 km, it was not possible to separate the coastline (shown in red in the satellite image) from the tsunami signal. Therefore, it is very likely that the upward spike in the Latitudinal Signal Diagram is a composite of the red coastline and of the tsunami signal.

The Longitudinal Signal Diagram, which is a slice of the Satellite Image along the longitude of the epicenter, is shown in Figure 10c. The position of the earthquake epicenter is marked by a flag. Again, it was not possible to distinguish the tsunami signal from the coastline. The difficulty is attributed to the fact that the earthquake affected a smaller ocean area very close to the shoreline.

Also noted is that while the earthquake took place at 06:34, the satellite image was taken at 06:39, just 5 minutes later. This should not present any difficulty since – according to our estimate - only 2 minutes would have been required for the colder water to reach the ocean surface when the tsunami was generated.

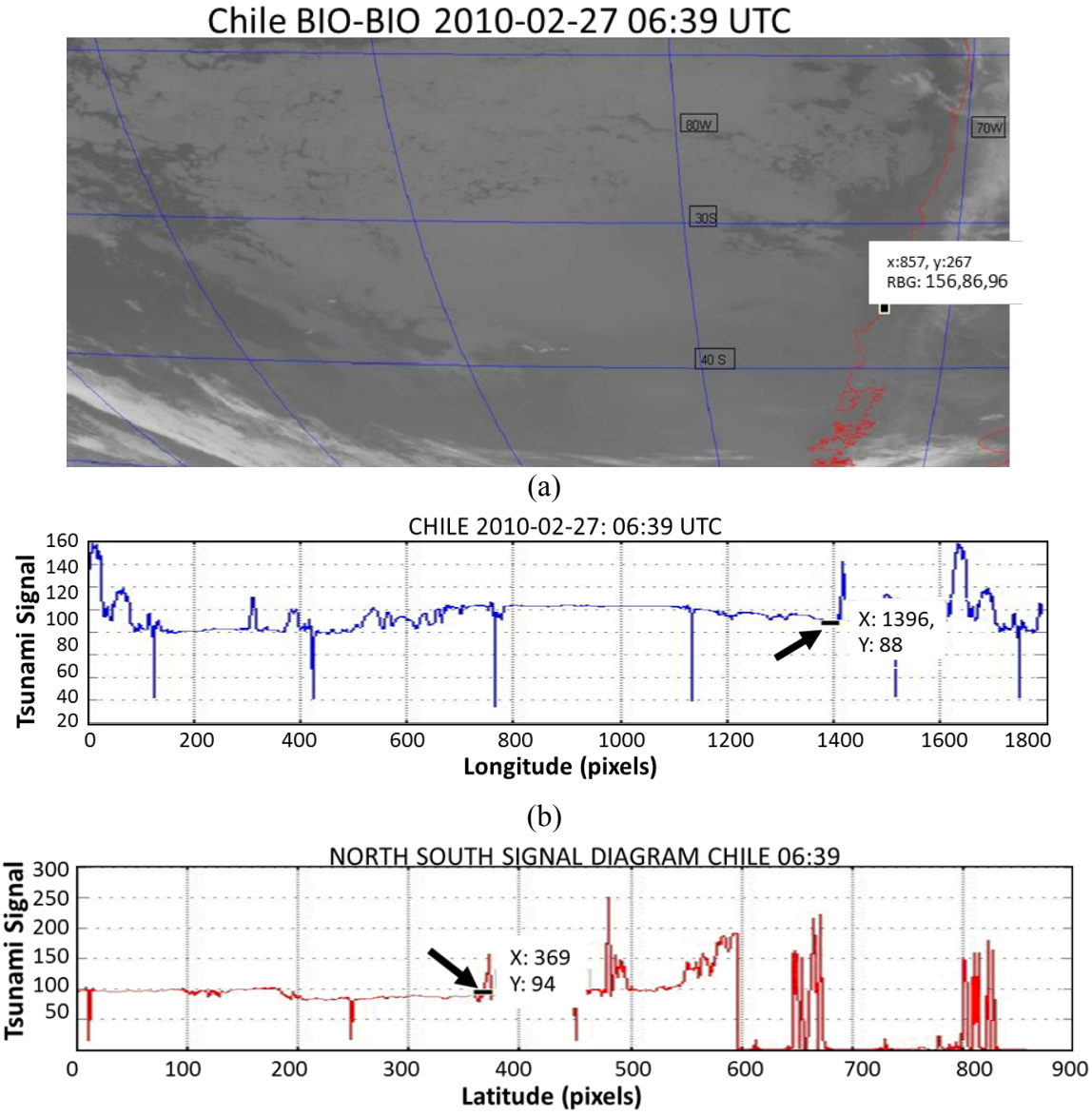

Fig. 10: Chile Bio-Bio earthquake event: a) Satellite image, b) Latitudinal Signal Diagram and c) Longitudinal Signal Diagram.

Additionally, in explaining the discrepancy, it should be mentioned that although it only takes about 4 minutes to receive a complete GOES image, the raw data reprocessed by NOAA before retransmitting it on 1691 MHz as WEFAX (Weather Facsimile) had a possible delay of about twenty minutes. The discrepancy of a recognizable tsunami signal reception could be due to this delay in transmission, as well as to the extreme land proximity of the submarine earthquake. Furthermore, it is

possible that the tectonic crustal movements affected the hydrodynamics of the rising water in this particular region and that the colder water deflected away from the ocean surface. Such deflection would be expected to have an influence on the strength of the thermal tsunami signal. However, further geological evidence may be needed to explain the signal anomaly for this particular event.

3.4 The 2012 Ofunato, Japan Tsunamigenic Earthquake

On December 7, 2012 at 08:18:24UTC another earthquake with moment magnitude 7.3 occurred east of Sendai, Japan. Its epicenter was at 37.9°N and 143.9°E and its focal depth was 36.1 km. The USGS reported that the earthquake resulted from reverse faulting within the oceanic lithosphere of the subducting Pacific plate moving west northwestward beneath Hokkaido and northern Honshu, Japan. A tsunami warning was issued immediately after the earthquake. A maximum wave of about 1 meter in height reached the Ayukawa district of Ishinomaki at 6:02 P.M. local time, but no casualties were reported.

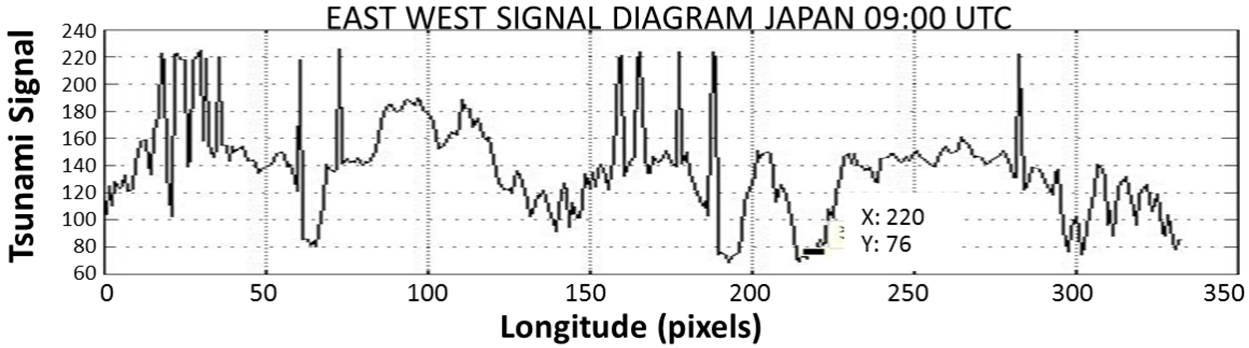

Fig. 11: Latitudinal Signal Diagram for Ofunato, Japan.

Figure 11 shows the latitudinal Signal Diagram taken at 09:00 UTC by MTSAT. At the location of the submarine earthquake, as marked by a flag, there is no evidence of tsunami signal. Since forty minutes elapsed between the earthquake and the satellite infrared exposure, the tsunami thermal signal would have been expected to have decayed. Curiously however, a radiation sink appears to be at the earthquake epicenter at that time.

In order to reduce the blind interval when the satellite image is being refreshed, it is possible to retain multiple geostationary satellites, such as the MTSAT-2 (which takes about 30 minutes to complete a scan) in addition to the FY-2x, whose periods do not overlap for the Asia-Pacific region. Furthermore, in case of an emergency when a strong submarine earthquake has been detected, the scanning interval can be reduced to 10 minutes instead of the customary 30 minutes, as implemented by the Russian satellite Elektro-L. This satellite is stationed over the Indian Ocean at 76°E longitude and can image the entire Earth hemisphere. Its resolution in the infrared band is 4 km. Sensor data downlink to ground uses an X-band (7.5 GHz.) frequency and offers data rates of up to 15.36 Mbits/s.

3.5 The 2012 Sulangan, Philippines Tsunamigenic Earthquake

On 2012-08-31 12:47:34 UTC an earthquake with moment magnitude of 7.6, epicenter at 10.8°N and 106.8°E and a focal depth of 34.9 km occurred 96 km east of Sulangan, Philippines. According to the USGS, this earthquake was an intraplate event, which resulted from reverse faulting within the oceanic lithosphere in the region between the Philippines Sea plate and the Sunda plate. Tectonically, the Philippine Sea plate is bounded by the larger Pacific and Eurasian plates and the smaller Sunda plate. At the latitude of the earthquake, the Philippines Sea plate moves west northwestward at a velocity of approximately 10 cm/year with respect to the Sunda plate.

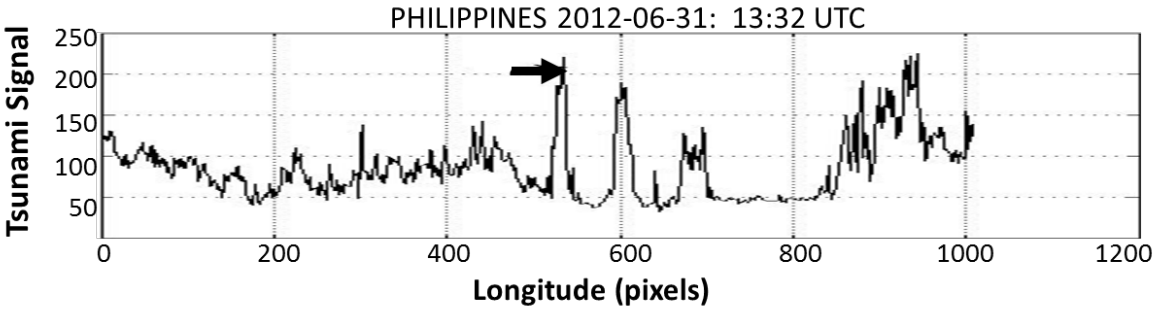

Fig. 12: Latitudinal Signal Diagram for Sulangan, 2012-08-31: 13:32.

Figure 12 shows the Latitudinal Signal Diagram taken by MTSAT on 2012-08-31 at 13:32 UTC. As pointed to by an arrow, the thermal tsunami signal is readily identifiable at the location of the earthquake. According to local authorities, about two hours after the quake, a series of small waves ranging up to 50 centimeters in height, struck the shores of the eastern Philippine Islands, but without causing major damage. There was a report of only one death from a landslide.

3.6 The 2012 Northern Sumatra Events

Clouds whose radiation in the infrared range may not be distinguishable from the tsunami signals frequently cover the world oceans. This constitutes the main source of noise in the detection of tsunamis by the described remote sensing method of the present study. However, it is possible to suppress this noise with an appropriate application of wavelet analysis. We show how utilizing as example the Northern Sumatra tsunami that occurred in 2012 can do this. The parameters of these two tsunami events are given in Table 3.

Table 3: Parameters of the Northern Sumatra Tsunamis of 2012-04-11.

Event	***Me***	Time (UTC)	Lat.	Long.	Thermal Signal at epicenter, pixels	***Mt***
Main-shock	8.6	08:38	2.31	93.0	203	7.665
Aftershock	8.2	10:43	0.77	92.4	138	7.108

For the case of the Aftershock in Table 3, the location of the submarine earthquake marked by a flag on the satellite image is shown in Figure 13a. The Chinese Meteorological Satellite FY-2E on 2011-4-11 captured the historical satellite image in Figure 13a immediately after the seismic events. The red lines are land boundaries; the blue lines are latitudes and longitudes. White patches outside the land mass are clouds over the ocean.

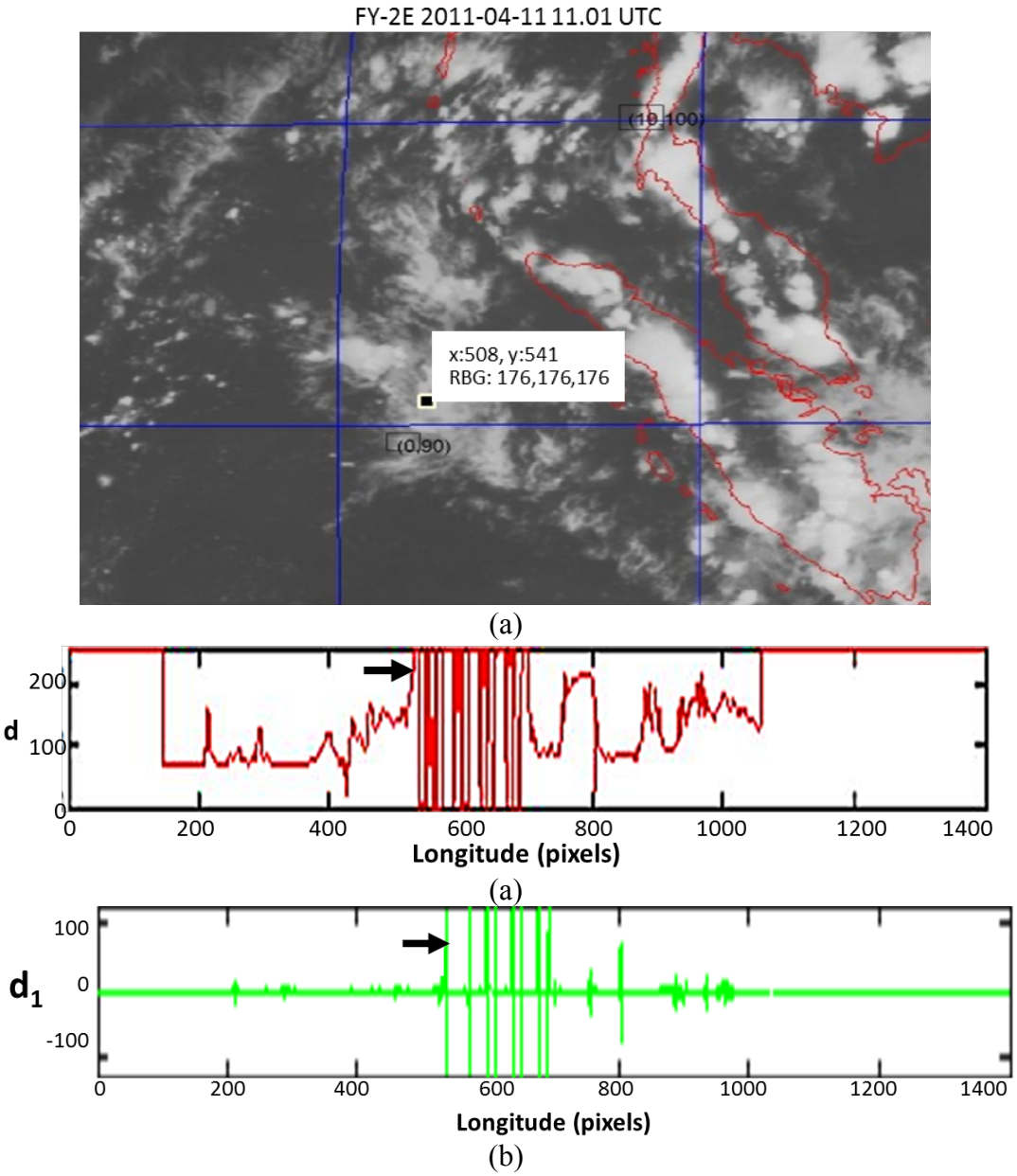

Fig. 13: North Sumatra aftershock at 11:01 UTC; a) Satellite image, b) Signal Diagram and c) Wavelet Diagram.

It is seen that while the cloud in the Signal Diagram, illustrated in Figure 13b, obscures the tsunami signal it is clearly distinguishable in the Wavelet Diagram, shown in Figure 13c. An arrow points to the location of the submarine earthquake. We observe that in Figure 13b the arrow points not to a sharp spike as we would expect from a tsunami signal, but to a block of closely packed, adjacent signals extending between 2 notches. This block is the superposition of the tsunami signal with the infrared radiation emanating from the cloud, which hovers over the location of the earthquake's epicenter. The white patches that are not over land mass - which is demarcated by red boundaries in the mapped image – are due to radiation from the cloud. It is seen from the satellite image that extensive cloud cover covers the location of the submarine earthquake. In the Wavelet Diagram the tsunami signal is clearly visible as a sharp spike at the location of the submarine earthquake. As mentioned earlier, this is because wavelet analysis can compress or denoise a signal without appreciable degradation. Also, it is possible that a cloud cover can be so dense that no infrared radiation can penetrate it. However, this does not happen very often. For instance, in the Indian Ocean during the monsoon season, the clouds are carried by the wind at considerable speed, so that any single cloud does not stay at one location long enough to obscure the tsunami signal.

Another source of noise is the infrared radiation emitted by the adjacent land mass. However, we can easily recognize its origin by comparing the satellite image with a topographic map. Regarding the horizontal scale, all Signal Diagrams encompass 500 pixels between notches and all Wavelet Diagrams span 200 pixels between notches unless otherwise labeled. For the vertical scale, the range of Signal Diagrams is from 0 to 250 and the range for Wavelet Diagrams is from -100 to +100, unless otherwise labeled.

4. DISCUSSION

In order to be able to assess the damage that can be caused by a tsunami and issue a warning as to the severity of its anticipated impact, it is useful to define a measure of tsunami magnitude and relate it to the severity of the submarine earthquake that generated it. In phase space, Iida *et al*. [Iida, 1958; Iida *et al*., 1967] defined the tsunami intensity by:

$$It = log2(\sqrt{2} \times S) \tag{1}$$

Where S is the estimated maximum run-up height of the wave. The logarithmic function is convenient, as in the case of the Richter scale, to compress the numerical values into a narrow range. This measure has also been suggested based on the effect and damage caused by the tsunami. In the following we shall consider three possible definitions of tsunami magnitude in infrared space. The Tsunami Magnitude, the Tsunami Index, and the Tsunami Coefficient. In analogy to equation (1), we define the *Tsunami Magnitude*, Mt as follows:

$$Mt = log2S \tag{2}$$

where Mt is *Tsunami Magnitude* and S represents *Tsunami Signal* (Pixel brightness at the epicenter. See Table 1 for numerical values obtained directly from the satellite images). Based mainly on empirical data, Iida *et al*. [Iida, 1958; Iida *et al.*, 1967] found a linear relationship between the Mt and Me in visible space, as follows:

$$Mt = 2.61Me - 18.44 \quad (3)$$

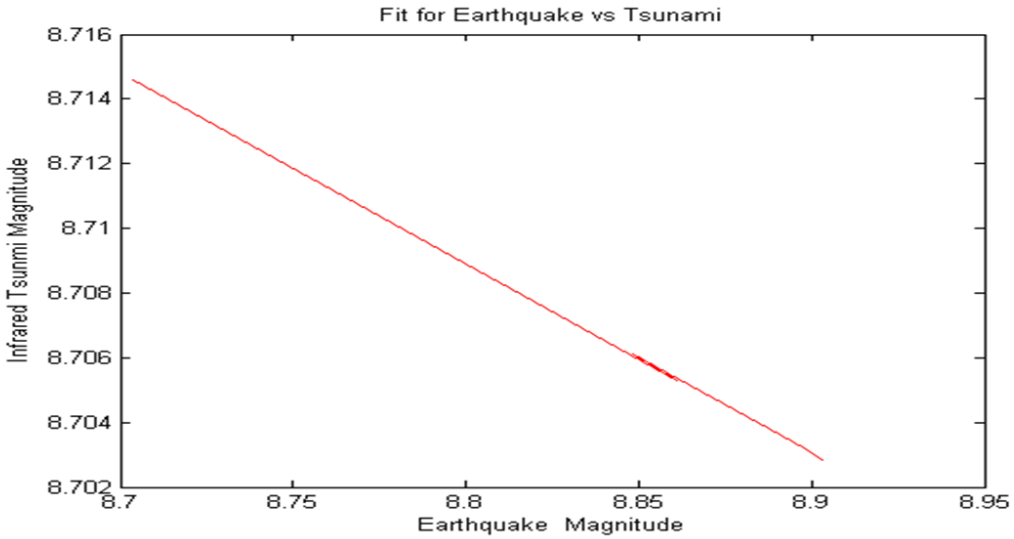

Fig. 14: Infrared tsunami vs earthquake magnitude.

As in the case of Iida *et al.* the earthquake magnitude and tsunami magnitude *in infrared space* also lie approximately on a straight line. The equation for least square fit is given by:

$$Mt = 9.2299 - 0.052Me \quad (4)$$

We observe that the Tsunami Magnitude as we have defined is a decreasing function of the earthquake magnitude as shown in Figure 14. This is probably a manifestation of the negative correlation between temperature and tsunami signal: the lower the temperature of the water, the stronger is the tsunami signal. However, in customary usage, this is counter-intuitive. Intuitively it is useful to regard a measure of tsunami magnitude as an increasing function of the earthquake magnitude. We define a calibrated tsunami magnitude called the *Tsunami Index*, I as follows:

$$I = 1000log2 - 1S - 110 \quad (5)$$

The relationship of I to Me is given in Fig. 15 for Banda Aceh:

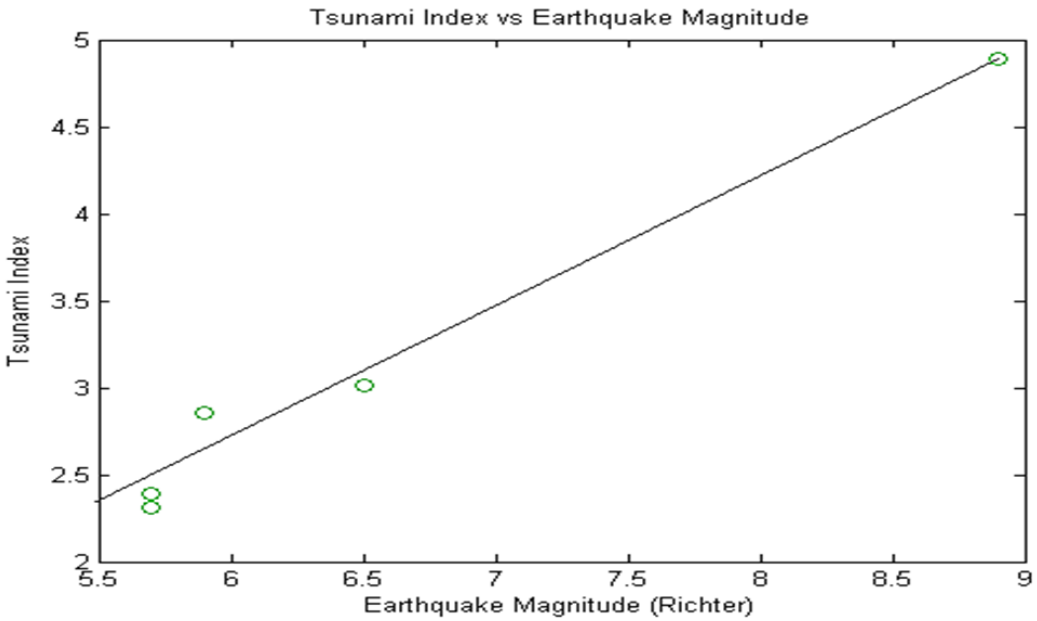

Fig. 15: Earthquake Magnitude (*Me*) vs Infrared Tsunami Index (*I*) at epicenter.

These results can be used to estimate the tsunami magnitude. The 'far point' in Figure 15 is the Main Event. As we have mentioned, there are many factors that contribute to the birth of a tsunami. Since in the range we are considering, the submarine earthquake is a *force majeure* [Lin and Sookhanaphibarn, 2011], other factors such as underwater currents are insignificant in comparison or cancel out.

The strength of a tsunami can also be estimated by the reciprocal of the Tsunami Signal. We define the Tsunami Coefficient, *K* as follows:

$$K = 1000S - 1 \tag{6}$$

An empirical formula between the *Tsunami Coefficient*, *K*, and the *Earthquake Magnitude* is given by equation (7) as follows.

$$K = 0.0922Me - 1.579 \tag{7}$$

from which we can estimate the tsunami strength from the earthquake magnitude, subject to the limitation of the approximations involved. The data points in Fig. 16 are from Banda Aceh. The goodness of fit is: *SSE* = 0.001 and *R-square* = 0.9839. We do not expect the linearity to be perfect, since the ocean floor bathymetric features vary greatly at different locations.

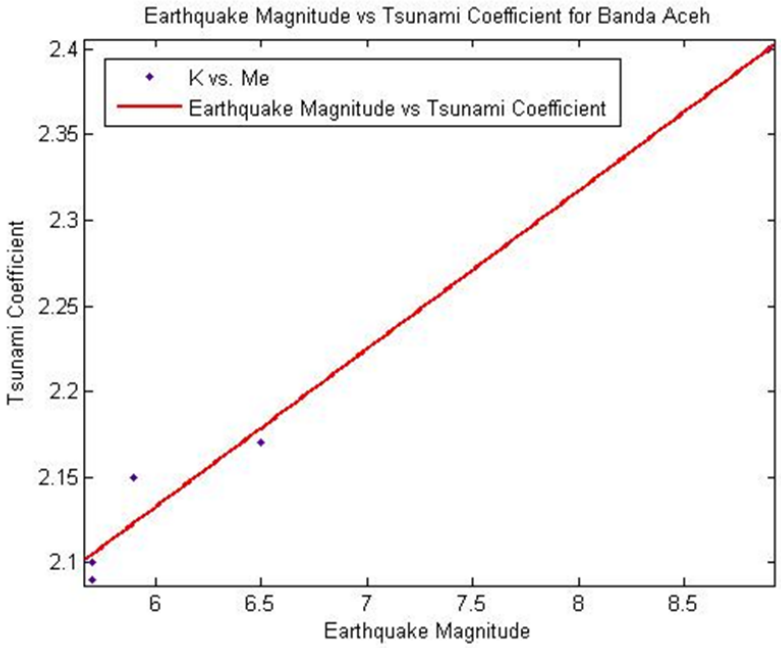

Fig. 16: Tsunami Coefficient (*K*) vs Earthquake Magnitude (*Me*).

Table 4: Tsunami Magnitude and Tsunami Coefficient.

Location	**Event**	***Me***	**Time UTC**	***S* pixels**	***K***	***Mt***
INDIAN OCEAN	Main- shock	8.9	00:58	417	2.40	8.7
	Aftershock	5.9	02:59	465	2.15	8.9
	Nicobar	6.5	09:20	461	2.17	8.8
	Andaman-1	5.7	07:07	477	2.10	8.9
	Andaman-4	5.7	06:21	479	2.09	8.9
TOHOKU	Main- shock	9.0	05:46	255	3.92	7.9
	Foreshock	7.2	02:45	197	5.08	8.0
	Aftershock-1	7.1	14:32	161	6.21	7.33
	Aftershock-3	7.9	06:15	255	3.92	8.0
N.SUMATRA	Main- shock	8.6	08:38	203	4.92	7.7
	Aftershock	8.2	10:43	138	7.25	7.1

As previously indicated, we have investigated thoroughly the tsunami phenomena in infrared space. Other investigators, such as the MOST model [Titov and Gonzalez, 1997], have made use of variables in phase space. The question that can be posed is: What is the relationship between these two representations? Since both representations stand for the same tsunami, it must be possible to map from one to the other by a mathematical transformation and since the dynamic equations are linear, by

a linear transformation. We construct a generalized hyperspace, in which both the phase space and the infrared space are embedded. The two representations are vectors in this space. We can therefore carry out a linear transformation to map an element from IR to P or vice versa by a rotation and two translations. Thus [Lin and Sookhanaphibarn, 2011]:

$$vp = \boldsymbol{R} \cdot vIR + \boldsymbol{T}Me \cdot vIR + \boldsymbol{T}Mt \cdot vIR \tag{8}$$

The matrix $\boldsymbol{R}$ is the usual rotational operator given by:

$$\boldsymbol{R} = \begin{matrix} \cos\varphi & -\sin\varphi & 0 \\ \sin\varphi & \cos\varphi & 0 \\ 0 & 0 & 1 \end{matrix} \tag{9}$$

where φ is the angle of rotation.

Therefore these representations are equivalent. If any other space is invoked, its elements must satisfy the condition that a linear transformation exists which maps its elements into the canonical representation, in order that the tsunami magnitude is self-consistent with the other representations.

This theorem is supported by experimental data, for instance by satellite data compared with the DART data of 2011-03-11 at Tohoku, as shown in Figure 9.

The quantity $\mathcal{S}$ in the Table 4 is the strength of the tsunami signal (pixel brightness). Since the earthquake and the tsunami signal are *causally related*, it could not have been a coincidence that they occupy the same point, i.e. same spatial position and the same time, in Minkowski space. We conclude therefore that the relation between them is not random.

5. CONCLUSION

In a previous communication [Lin *et al*., 2013] we have shown the advantages of the REMOTE system as a satellite based tsunami early warning system. In the following we discuss the performance features of REMOTE from four points of view: Time delay, reliability, cost and availability. In terms of time delay, assuming that the depth of submarine earthquake is 30 km and the velocity of the tsunami is 1000 km/hr, it will take 2 minutes for the tsunami signal to reach the geostationary satellite and a warning broadcasted. *This time lapse is critical for the effectiveness of Early Warning*. In terms of cost, we estimate that the initial cost including hardware and software will be of the order of 10^4 euros and the maintenance cost is minimal. For private entrepreneurs, it is possible to purchase the components of our system via the Internet for a few hundred euros.

For our system, in theory, there are no false positives or false negatives. It is easy to understand this if we consider two cases: 1) The cool water from the bottom of the ocean is dissipated before it reaches the surface. 2) The cool water reaches the surface of the ocean, mixes with warm water, and radiates. In the first case, no tsunami is generated and the satellite did not detect the tsunami signal. It

is a negative event. In the second case, the satellite does receive a tsunami signal and therefore sounds a warning. It is a positive event (In our catalog the Chile Bio-Bio is an ambiguous case due to its unusual topology). In terms of availability, this system can be made available to every country with access to a weather satellite. If implemented, this system should function essentially instantaneously without any margin of error, and should benefit all communities presently threatened by tsunamis, thereby saving life and property.

REFERENCES

M. Arii, M. Koiwa, and Y. Aoki, "Effective monitoring for marine debris after the great east Japan earthquake by using polarimetric SAR data," IGARSS 2013, Melbourne, Australia, Jul. 2013.

E. Bernard and C. Meinig, "History and future of deep-ocean tsunami measurements," in OCEANS 2011, pp. 1-7, 2011.

J.-F. Cayula and P. Cornillon, "Edge detection algorithm for SST images," Journal of Atmospheric and Oceanic Technology, vol. 9, no. 1, pp. 67- 80, 1992.

L. H. Coudert, O. Pirali, M. Vervloet, R. Lanquetin, and C. Camy-Peyret, "The eight first vibrational states of the water molecule: measurements and analysis," Journal of Molecular Spectroscopy, vol. 228, pp. 471- 498, December 2004.

E. L. Geist, V. V. Titov, D. Arcas, S. L. Bilek, and F. F. Pollitz, "Implications of the 26 December 2004 Sumatraandaman earthquake on tsunami forecast and assessment models for great subduction-zone earthquakes," Bulletin of the Seismological Society of America, vol. 97, pp. S249-S270, January 2007.

F. Gonzalez, "Tsunami!," Scientific American, vol. 280, pp. 56-65, 1999.

B. D. Hamlington, R. R. Leben, O. A. Godin, J. F. Legeais, E. Gica, and V. V. Titov, "Detection of the 2010 chilean tsunami using satellite altimetry," Natural Hazards and Earth System Science, vol. 11, no. 9, pp. 2391-2406, 2011.

B. Hamlington, R. Leben, O. Godin, E. Gica, V. Titov, B. Haines, and S. Desai, "Could satellite altimetry have improved early detection and warning of the 2011 Tohoku tsunami?," Geophysical Research Letters, vol. 39, no. L15605, 2012.

K. Iida, "Magnitude and energy of earthquakes accompanied by tsunami and tsunami energy," Journal of Earth Science, vol. 6, no. 2, pp. 101- 112, 1958.

K. Iida, D. C. Cox, and G. Pararas-Carayannis, "Preliminary catalog of tsunamis occurring in the Pacific Ocean," Hawaii Institute of Geophysics, University of Hawaii, 1967.

F. C. Lin and I. E. Mohamed, "Predicting seismic aftershocks using a neural network," in Proceedings of the IEEE 1999 International Geoscience and Remote Sensing Symposium, vol. 2 of IGARSS99, (Munich, Germany), pp. 1366-1368, July 1999.

F. C. Lin, N. Elhassan, A. Hassan, and A. Yousif, "Forecast of seismic aftershocks using a neural network," in Proceedings of the 9th International Conference on Neural Information Processing, 2002, vol. 4 of ICONIP'02, (Singapore), pp. 1796-1799, July 2002.

F. C. Lin, K. n. Nakornphanom, K. Sookhanaphibarn, and C. Lursinsap, "A new paradigm for detecting tsunamis by remote sensing," International Journal of Geoinformatics, vol. 6, no. 1, pp. 19-30, 2010.

F. C. Lin and K. Sookhanaphibarn, "Representation of tsunamis in generalized hyperspace," in Proceeding of the IEEE International Geoscience and Remote Sensing Symposium, IGARSS11, (Sendai/Vancouver), pp. 4355-4358, July 2011.

F. C. Lin, W. Zhu, and K. Sookhanaphibarn, "Observation of tsunami radiation at Tohoku by remote sensing," Science of Tsunami Hazards, vol. 30, no. 4, pp. 223-232, 2011.

F. C. Lin, W. Zhu, and K. Sookhanaphibarn, "A detail analysis of the Tohoku tsunami by remote sensing," in Proceedings of the IEEE International Geoscience and Remote Sensing Symposium, IGARSS12, (Munich, Germany), pp. 1166-1169, July 2012.

F. C. Lin, W. Zhu, P. Silapasuphakornwong, and K. Sookhanaphibarn, "Remote: a satellite based tsunami early warning system," in Proceedings of the IEEE 2013 International Geoscience and Remote Sensing Symposium, IGARSS13, (Melbourne, Australia), pp.3694-3697, July 2013.

G. Pararas-Carayannis, "The Great Tohoku-Oki Earthquake and Tsunami of March 11, 2011 in Japan: A Critical Review and Evaluation of the Tsunami Source Mechanism," Pure and Applied Geophysics, pp. 1-22, 2013.

J. Park, K. Anderson, R. Aster, R. Butler, T. Lay, and D. Simpson, "Global seismographic network records the great Sumatra-Andaman earthquake," Eos, Transactions American Geophysical Union, vol. 86, no. 6, pp. 57-61, 2005.

J. Park, K. Anderson, R. Aster, R. Butler, T. Lay, and D. Simpson, "A catalog of tsunamis in the Indian ocean," Science of Tsunami Hazards, vol. 25, no. 3, pp. 128-142, 2006.

D. B. Percival and A. T. Walden, Wavelet Methods for Time Series Analysis (Cambridge Series in Statistical and Probabilistic Mathematics). Cambridge University Press, Feb. 2000.

V. V. Titov and F. I. Gonzalez, “Implementation and testing of the method of splitting tsunami (most) model,” tech. rep., NOAA Technical Memorandum ERL PMEL-112, 11 pp UNIDATA, 1997.

C. E. Synolakis, E. N. Bernard, V. V. Titov, U. Knoglu, and F. I. Gonzlez, “Validation and verification of tsunami numerical models,” Pure and Applied Geophysics, vol. 165, pp. 2197-2228, 2008.

P. C. C. Ullman, David S., “Evaluation of front detection methods for satellite-derived SST data using in situ observations,” Journal of Atmospheric and Oceanic Technology, vol. 17, pp. 1667-1675, 2000.

ISSN 8755-6839

SCIENCE OF **TSUNAMI HAZARDS**

Journal of Tsunami Society International

Volume 33 **Number 2** **2014**

VALIDATION OF THE JRC TSUNAMI PROPAGATION AND INUNDATION CODES

N. Zamora
GeoForschungsZentrum (GFZ), Germany

G. Franchello and A. Anunziato
EC-Joint Research Centre (JRC), Italy

ABSTRACT

In the last years several numerical codes have been developed to analyse tsunami waves. Most of these codes use a finite difference numerical approach giving good results for tsunami wave propagation, but with limitations in modelling inundation processes. The HyFlux2 model has been developed to simulate inundation scenario due to dam break, flash flood and tsunami-wave run-up. The model solves the conservative form of the two-dimensional shallow water equations using a finite volume method. The implementation of a shoreline-tracking method provides reliable results. HyFlux2 robustness has been tested using several tsunami events. The main aim of this study is code validation by means of comparing different code results with available measurements. Another objective of the study is to evaluate how the different fault models could generate different results that should be considered for coastal planning. Several simulations have been performed to compare HyFlux2 code with SWAN-JRC code and the TUNAMI-N2. HyFlux2 has been validated taking advantage of the extensive seismic, geodetic measurements and post-tsunami field surveys performed after the Nias March 28th tsunami. Although more detailed shallow bathymetry is needed to assess the inundation, diverse results in the wave heights have been revealed when comparing the different fault mechanism. Many challenges still exist for tsunami researchers especially when concern to early warning systems as shown in this Nias March 28th tsunami.

Keywords: *fault scenarios, tsunami propagation, HyFlux2 code.*

Vol. 33, No. 2, page 112 (2014)

1. INTRODUCTION

Tsunami wave propagation has been an important focus of study since the significant studies of Mader (1974). In the last two decades many numerical code have come to light using different numerical approaches. Developers have improved robustness by testing different numerical methods. Moreover, seismological data and tsunami surveys have helped to validate the reliability of these codes with the important application coastal planning and tsunami early warning.

A mega-thrust earthquake magnitude 8.6 occurred on March 28th, 2005 with epicentre at Nias Island at 16:10:31 UTC (around 110 km to the SE of the 12/26/2004 earthquake). The earthquake triggered a tsunami with maximum 3 m run-up at Simeulue Island, a 2 m run-up at Nias Islands and 1 m Singkil and Meulaboh in Sumatra Main Island. Red tsunami alert was sent by the European Commission Global Disaster Alert and Coordination System (GDACS) 16 minutes after the event. The Joint Research Centre of the European Commission (JRC) has developed different types of tsunami calculations such as the near-real time calculations, the grid scenarios calculations and the post event calculations. When a new event is detected by the seismological sources (e.g. USGS, EMSC), an evaluation is performed to estimate the importance of the event from humanitarian point of view. This is important for the needs of alert systems. Fault models, their selection and the best automatic process for alerting systems have been a great challenge. Slip distribution is one of the main inputs for a reliable tsunami numerical simulation this research intends to evaluate different fault models and also numerical code performance. Besides, improvement of alerting systems has driven to consider the applications of Global Positioning Systems (GPS) into tsunami early warning systems since they can measure ground motions in real time every few seconds (Sobolev et al., 2007; Song, 2007; Falck et al., 2010). The measurements from GPS in buoys could allow an almost real-time detection of tsunami waves offshore. This offshore data attached with onshore GPS that determines ground movements are of great importance and started to be implemented (Falck, 2010). Implementation of such new methods joined with actual fault mechanism analysis could address to acquire more reliable deformation data in near real-time-earthquake occurrence. However, up to now this information is not integrated in GDACS retrieving systems or databases that consider seismological data available.

Therefore, near field tsunami events are an important source to assess the accuracy of ground deformation models which provides the input of the hydrodynamic models. Given that an important amount of scientific data is available from post-event field surveys, geodetic measurements and seismological data, we have the aim to make an evaluation of the tsunami propagation and inundation numerical codes used at the JRC.

We present comparisons of several post-event calculations done with three different numerical codes. In addition, fault scenario tsunami inundation differences along the coast are evaluated. Simulations have been performed to compare the results obtained by the SWAN-JRC code (Annunziato, 2005; 2007), the TUNAMI-N2 (Imamura, 2006) and the HyFlux2 (Franchello, 2008). The event was simulated by defining the initial conditions by means of the Finite fault model (Ji et al, 2002) and the fault solution of Okada Fault Model using the Global Harvard Moment Tensor solution (gCMT).The Northern Sumatra earthquake (Nias event) is a good example to understand and to evaluate the

performance and reliability of these numerical codes in earthquakes occurring very close to the coast and in which tsunami alert is a challenge due to the small time available to alert communities.

As has been known from historic data and recent events, this region is a prone area for generation of earthquakes and tsunamis. Sunda region is a typical island-arc structure with a deep oceanic trench, a volcanic inner arc and a marginal basin. This region is one of the most seismically active regions in the world owing to the confluence of multiple plates moving at high relative speeds (McCaffrey, 2009).The rate of subduction varies along the trench being 5.9 cm/yr in South Sumatra and 5.3 cm/yr along the Indo-Australian plate subducting beneath Burma and Sunda plate (Prawirodirdjo and Bock, 2004; Subarya et al., 2006). In the last 35 years, 12 earthquakes with magnitudes greater to M*w* 7.4 have occurred along western Indonesia (Fig. 1.1).

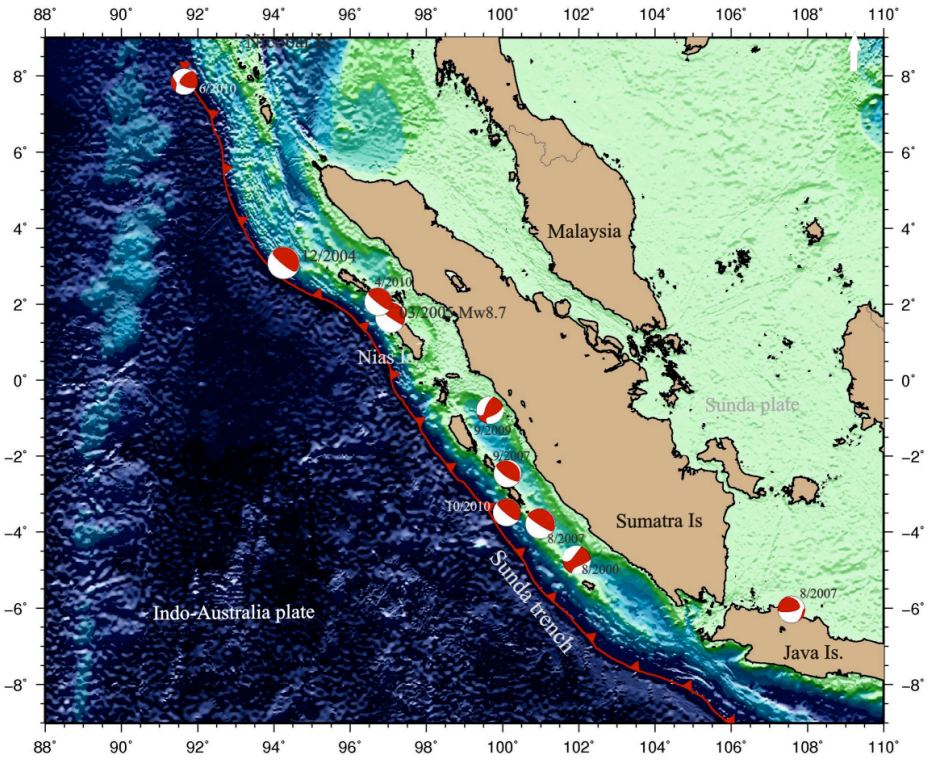

Figure 1.1. Sunda trench and gCMT earthquakes Mw>7.4 from 01/1976 - 01/2012.

2. CODES AND METHODS

Numerical approaches when apply to tsunami modeling have advantages and disadvantages concerning their applications to wave propagation, inundation or risk management. For further discussion about differences of numerical codes refers to Castro et al. (2012). Herein, we consider three numerical codes available at EC-JRC. The numerical codes SWAN-JRC, TUNAMI-N2 and HyFlux2 solve the shallow water equations using different numerical methods: SWAN and TUNAMI use the finite different method (FDM) while HyFlux2 uses the finite volume (FVM).

The shallow water equations are commonly used to describe tsunami wave propagation and general features of the inundation processes. These equations can be derived using different approximations, all of which relies on the assumption that the flow is vertically hydrostatic, the vertical velocity and the vertical acceleration are negligible. The fluid is incompressible, the water temperature is constant and the pressure at the free surface is constant.

The *SWAN-JRC code* (Annunziato, 2007) solves the shallow water equations by the finite difference numerical scheme based on SWAN Mader code (1988). This code has been implemented for *Global Disaster Alerts and Coordination System (*GDACS). The SWAN-JRC code estimates the fault length, height and direction to determine the initial water displacement. The code initializes the calculation space, performs the travel time propagation calculation, verify at each step if there are locations reached by the wave and thus update the visualization and animation files. For early warning purposes of GDACS the model can run in automatic mode and publish automatically the results in the GDACS web site. For post event calculations the Global Centroid Moment Tensor solutions (gCMT) and Finite Fault Model (FFM) as well as other earthquake parameters can be used to compare or improve simulation results.

The *TUNAMI-N2 code* was developed by the Disaster Control Research Center through the Tsunami Inundation Exchange Modeling (TIME) Program (Goto et al., 1997). It is based on the shallow water equations solved by a finite difference numerical scheme. The TUNAMI code consists of several codes. However in this project we have used the TUNAMI-N2 (linear theory in deep sea, non-linear shallow-water theory in shallow sea and run-up on land with constant grids). In this analysis TUNAMI-N2 has been used. TUNAMI-N2 code is included in the JRC Tsunami suite and therefore the results can be easily produced with the same environment as the SWAN code (Annunziato, 2005).

The HyFlux2 model has been developed to simulate severe inundation scenario due to dam break, flash flood and tsunami-wave run-up. The model solves the conservative form of the two-dimensional shallow water equations using a finite volume method. The interface flux is computed by a Flux Vector Splitting method for shallow water equations based on a Godunov-type approach. A second-order scheme is applied to the water surface level and velocity. Physical models are included to deal with bottom steps and shorelines. The second-order scheme together with the shoreline-tracking method makes the model well balanced in respect to mass and momentum conservation laws, providing reliable and robust results (Franchello, 2010). In relation to ground deformation mass conservation both the bathymetry change and sea level change must be applied. In HyFlux2 it is assumed an instantaneous and equal deformation applied for bathymetry and water level.

The coastal flooding and inundation are commonly simulated by extending propagation calculations perform with a nested grid approach. The code requires as input detailed information on seismic source mechanisms, gridded bathymetric data for the open sea propagation, and a set of gridded Digital Elevation Models (DEM) containing detailed bathymetry and topography in order to model the inundation phase. The most common procedure to track movements of the shoreline (Imamura, 1996; Liu et al., 1998; Imamura et al., 2006) is the moving boundary treatment. Run-up is calculated with nonlinear computations. The numerical codes such as TUNAMI-N2, among others, use the

moving boundary approach in inundation quantification. In contrast, HyFlux2 uses a shoreline tracking method to model the interface between dry and wet. The inundation 2D scheme of HyFlux2 has been designed to identify the shoreline as intersection between two planar surfaces which describe the bottom and the water free surface (Franchello, 2010).

Using those available numerical codes we first, analyzed two rupture models (gCMT and FFM) compared with field data and geodetic measurements (e.g InSAR). In a second step, fault model is used to evaluate tsunami propagation by means of three numerical codes. At last, inundation is calculated using HyFlux2 code. Different bathymetry resolutions have been used. In order to reduce the calculation time, early warning system requires a rather coarse resolution (> 2.6 min). Resolutions of 0.5' are also used to evaluate propagation results. In one case 0.1' resolution has been used to compare wave heights with field measurements. HyFlux2 is included in the suite of codes that can be called upon by the JRC Tsunami suite, allowing an easy comparison of the code results (Zamora et al., 2011).

3. RESULTS AND DISCUSSION

3.1 Fault models

Fault parameters as initial condition in tsunami modeling are one of the major factors that determine the wave propagation and distribution of run-up along the coast. Therein the adopted approaches to estimate the initial conditions are based on algorithm that calculates analytical solution for surface deformation in an elastic half-space (Okada, 1985). This algorithm estimates the distribution of coseismic uplift and subsidence by using the hypocenter of the earthquake, strike, dip, rake and average displacement of the fault. The other approach is based on calculation of slip distribution by separating the fault plane into sub-faults (Ji et al., 2002).

In order to perform reliable tsunami simulations it is necessary to determine best fit fault models describing hypocenter, length and width of the fault, slip distribution and fault mechanism. The selection of the best fault model is especially hard in tsunami early warning context. This has driven to the need for evaluating fault mechanism for the March 28th, 2005 and to perform numerical codes performance comparisons using (1) the Harvard Global Centroid Moment Tensor (gCMT strike 329°, dip: 8°, rake: 109°), available few minutes to hours after the event and (2) the USGS Finite Fault Model (Ji et al., 2002) available few days after the event (Fig. 3.1).

InSAR deformation measurements for Nias earthquake show two main slip patches along Simeulue and Nias islands with maximum coseismic uplift of 2.5 m (Briggs et al., 2009). However, the FFM and gCMT parameters resulted in coseismic distribution overestimation in the case of FFM and subestimation of coseismic deformation when using gCMT parameters. Maximum vertical deformation calculated when using gCMT parameters is in agreement with InSAR 2.5 m (Fig. 3.1a). At the eastern part of Nias Island subsidence have been reproduced with the gCMT fault model, however with the InSAR measurements, uplift in the range of 0.5 m – 1.0 m is indicated exactly at Nias Island (Fig. 3.1). Comparably, subsidence is resulted for most of Nias Island when using FFM.

Vertical deformation is not consistent with InSAR measurement along Batu and Banyaks Islands, between Simeulue Island and Nias Island. At the eastern part of the Batu and Banyak Island subsidence has been estimated with FFM. However, this pattern is not consistent according to InSAR measurements (Fig. 3.1b). The static displacement field on the surface predicted by FFM is up to 3 m for uplift (Fig. 3.1b). Finally, the coseismic vertical deformation between the two fault scenarios differs in 1 m. If InSAR assessment is used as the base to compare deformation areas, main slip is very different for the two fault scenarios (gCMT and FFM). These results have important implication for tsunami early warning systems.

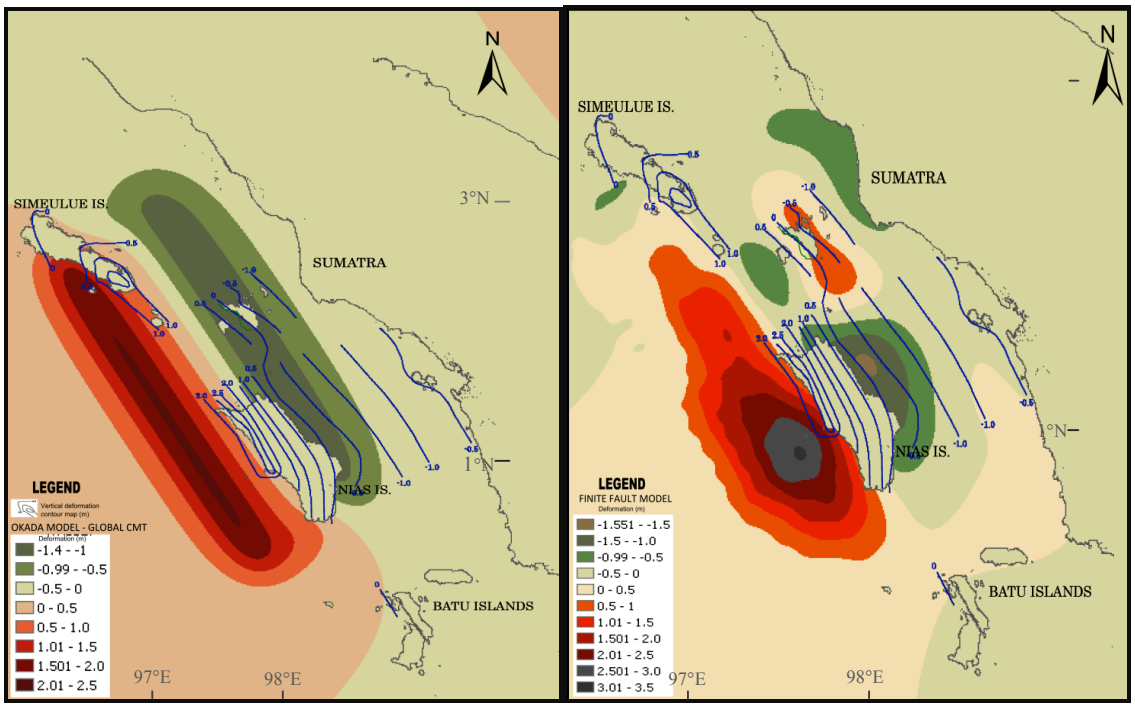

Figure 3.1. a. Resulted deformation using gCMT parameters in Okada Model. b. Fault deformation using FFM. The measured vertical deformation is shown by blue contours (from Briggs et al., 2009).

3.2 Calculation of wave using different fault models

It has been recognized that different hypocenter and slip distribution influence wave heights distribution along the coast. Therefore, simulations with gCMT model and FFM were performed to assess this difference wave heights resulted with SWAN-JRC simulations. Bathymetry grid of 900 m spatial resolution was used in these calculations.

The following map presents the location of the points where sea level is compared with the different fault models. At point S1 (behind Nias Island) amplitudes are very similar for both fault scenarios

(Fig. 3.2). At the S3 offshore point there is a small difference in time arrival of the first peak when comparing sea level trends resulted from the use of gCMT or Finite Fault Model. Because of location of point offshore the directivity and slip distribution is not affecting and therefore amplitudes are very similar on both fault models used in these simulations (Fig. 3.3).

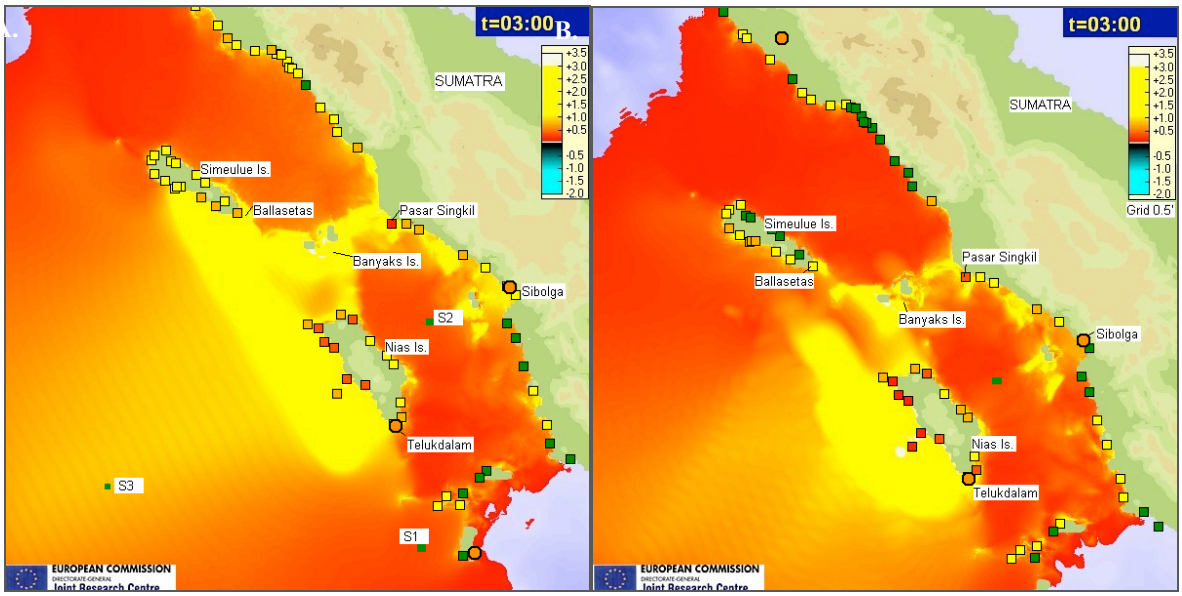

Figure 3.2. Maximum sea level resulted from simulations using two fault models a. Okada Model b. Finite Fault Model.

Arrival time of wave peak simulated using FFM is very similar when comparison is done at sites S1, S2 and S3 with offshore depths between -480 up to -4426 m (Fig. 3.4a). It is seen that most of the offshore directivity of wave is S-SW for FFM and SW for calculations performed using Okada model (Fig. 3.2).

Close to Ballesetas and Pasar Singkil the sea level trends differ for more than 1 m (Fig. 3.4b). This is related to the wave directivity caused by the fault orientation and by the slip patches (assessed by FFM). As expected, different focal mechanism and slip distribution resulted from Okada Model affect the initial wave profile. In addition, strike-directed slip variations could resulted in wave front-parallel changes in amplitude that are largely preserved during propagation from the source region toward shore causing refraction (Geist and Dmowska, 1999).

The following map shows a comparison of wave heights at selected coastal points (Fig. 3.. Wave height at these points were defined in a post processing step where the maximum wave height is acquired from a radius of 300 m to 1 km and for water depths close to 20 m. The main wave height differences at the shore are seen at Nias Island. This is related to slip coseismic distribution of each fault model.

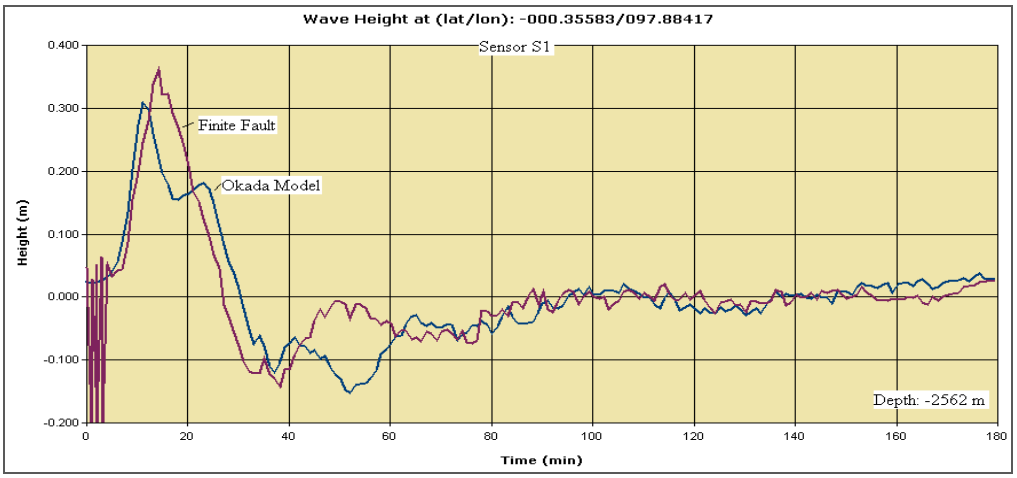

a. Comparison of wave heights offshore simulated with SWAN-JRC using two different fault models.

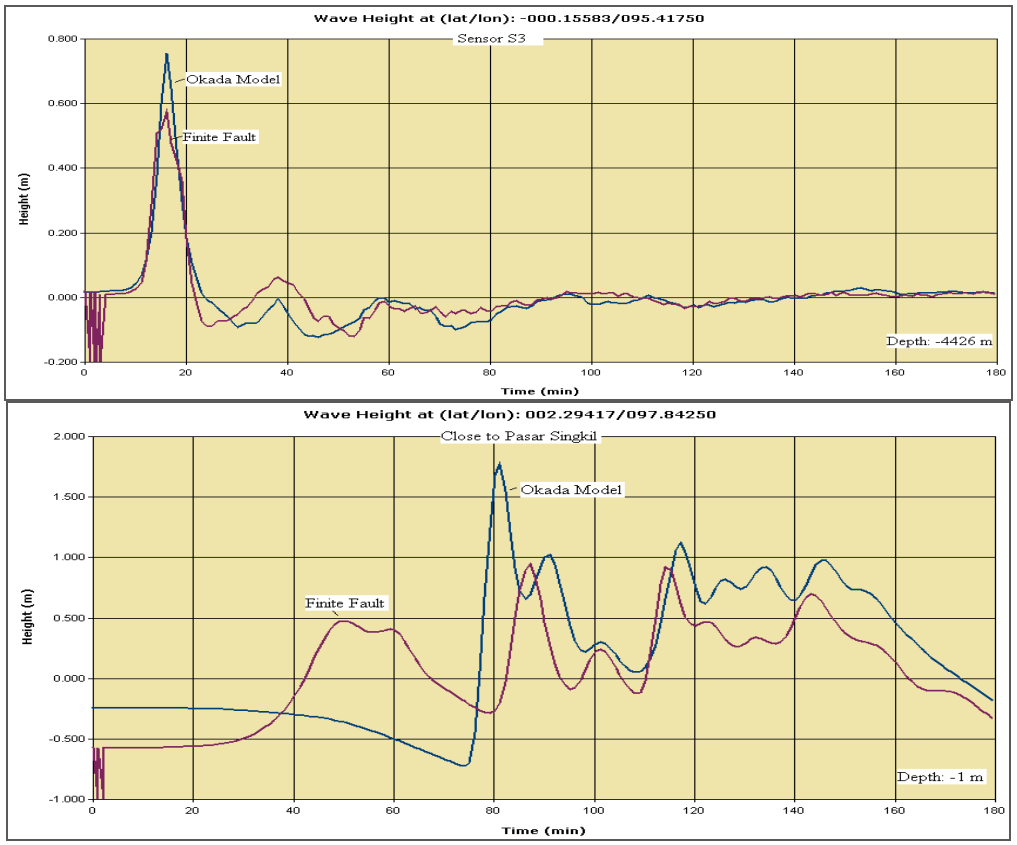

Figure 3.3.b. Comparison of wave heights close to shore. Simulations with SWAN-JRC using two different fault models.

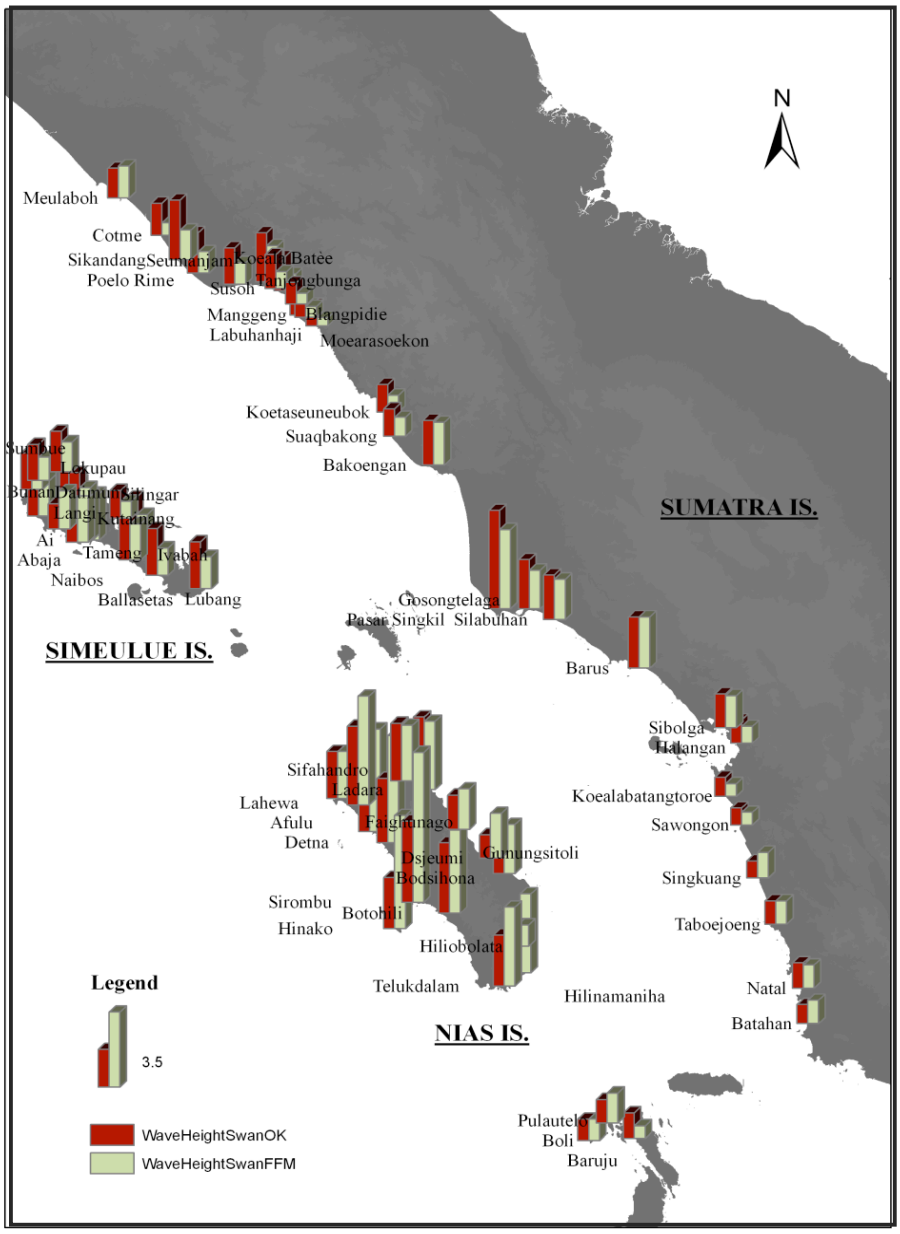

Figure 3.4. Maximum wave height resulted from 900 m bathymetry grid.

These differences in simulated wave height versus registered ones are related to the seafloor deformation characteristics (determination of fault mechanism), as observed especially for Nias Island where coseismic distribution from west to east varies from 1.5 m to -1.5 m on FFM and 1m uplift to -1.0 m east of Nias gCMT used on Okada Model.

3.3 Code to code assessment at 900 m resolution based on gCMT fault model

Sea level trends simulated at offshore (S2) point and at two sites close to shoreline are presented (Fig. 3.5). The objective is to compare wave height differences when using SWAN-JRC, HyFlux2 and TUNAMI-N2 numerical codes with gCMT parameters as input data. The calculation grid is 900 m. The maximum wave height recorded on simulation in point close to Telukdalam (Nias) arrives 11 minutes and 14 minutes after the earthquake according to SWAN-JRC and HyFlux2 respectively. At this point maximum wave height is 1.3 m (Fig. 3.5).

HyFlux2 code presents a smoother trend and differs for 3 minutes on first arrival compared to SWAN-JRC and TUNAMI-N2.

At location S2 the wave peak was recorded by SWAN-JRC code 18 minutes after the event. HyFlux2 code calculations registered the maximum height and first arrival at this point also 18 minutes after the event. Simulation with TUNAMI-N2 registered a wave 30 minutes after the event. Unfortunately no buoys were available to compare with real-time data.

As could be observed, HyFlux2 code results in shallow water do not show oscillations like the other codes. The smoother results can be due to the shoreline tracking method adopted in HyFlux2. In this sense, it is necessary to explain that HyFlux2 can provide 3 different values when performing simulations. These values are the maximum value of water height offshore (depth deeper than 20 m); the maximum value at shore (looking radius were determined from 300 m to 1 km along the shoreline) and the value inland. The more detailed bathymetric and topographic resolution, the smaller the radius on the coast needed for comparison and will drive to more reliable results for inundation assessment.

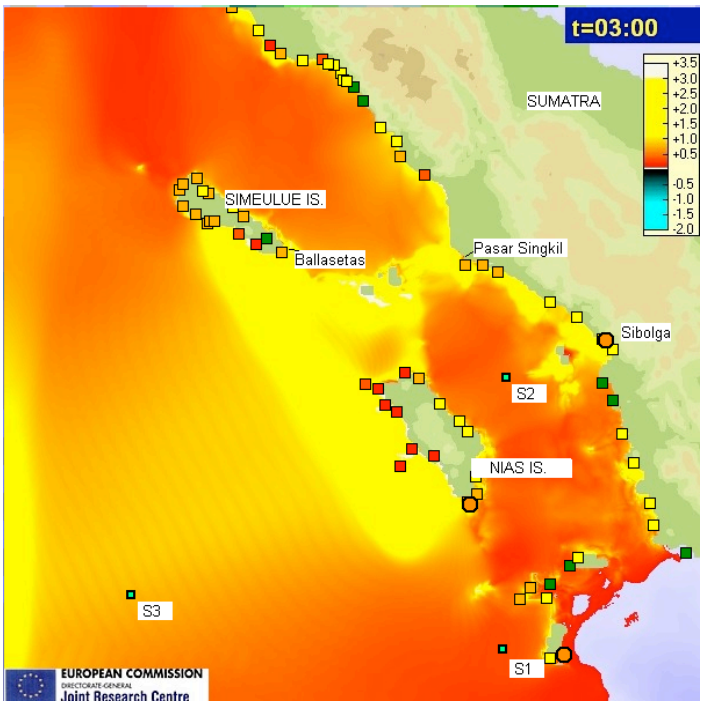

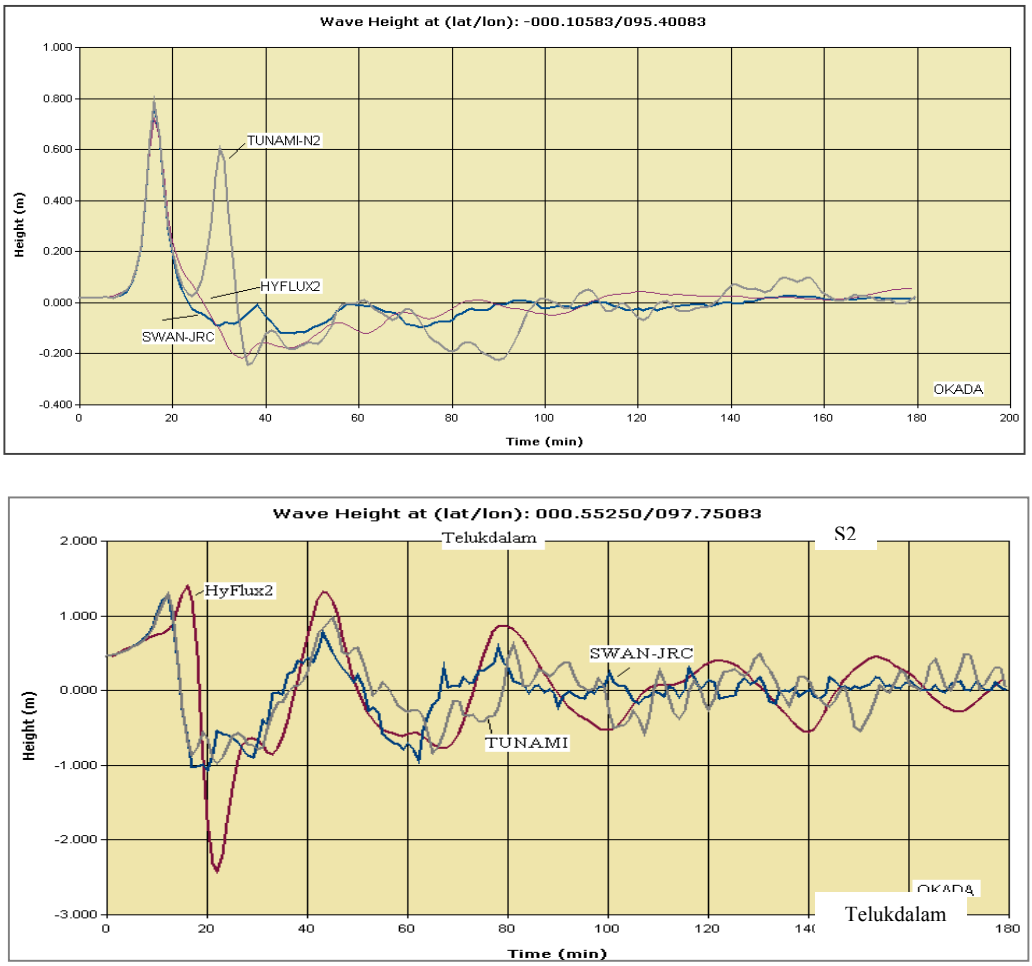

Figure 3.5. Maximum sea level resulted from HyFlux2 simulation using Okada Model.

From the sea level profiles shown above it has been concluded that the three numerical codes have similar behavior offshore. This does not apply when comparing HyFlux2 results with SWAN-JRC at very shallow waters sites, where the ratio (0.76)[1] of wave heights show wave heights with lower values HyFlux2 calculations. The ratio of HyFlux2 code calculations compared to TUNAMI-N2 is 0.6. Despite the fact that we tested that when wave heights simulated with HyFlux2 codes seem to be subestimated perhaps because we are using wave heights at shore. Moreover, when the so called zmaxShore (Fig. 3.6) provided by HyFlux2 post-processing is compared to the values given by SWAN-JRC, the ratio tend to be similar 1.11 (Fig. 3.8).

[1] The ratio has been calculated by AVERAGE[*wave height location values HyFlux2 code/ wave height location values SWAN-JRC*].

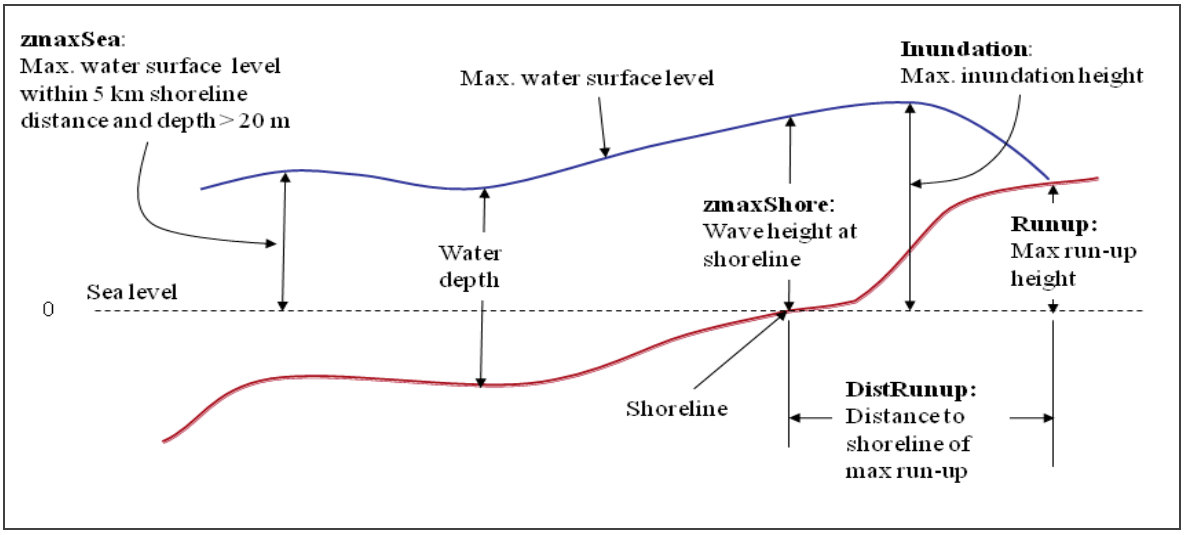

Figure 3.6. Sketch with definition of considred measurements (Franchello and Annunziato, 2012).

In the following maps wave height comparison of three codes is presented. This wave heights represented on the map are those resulted on heights higher than 0.5 m.

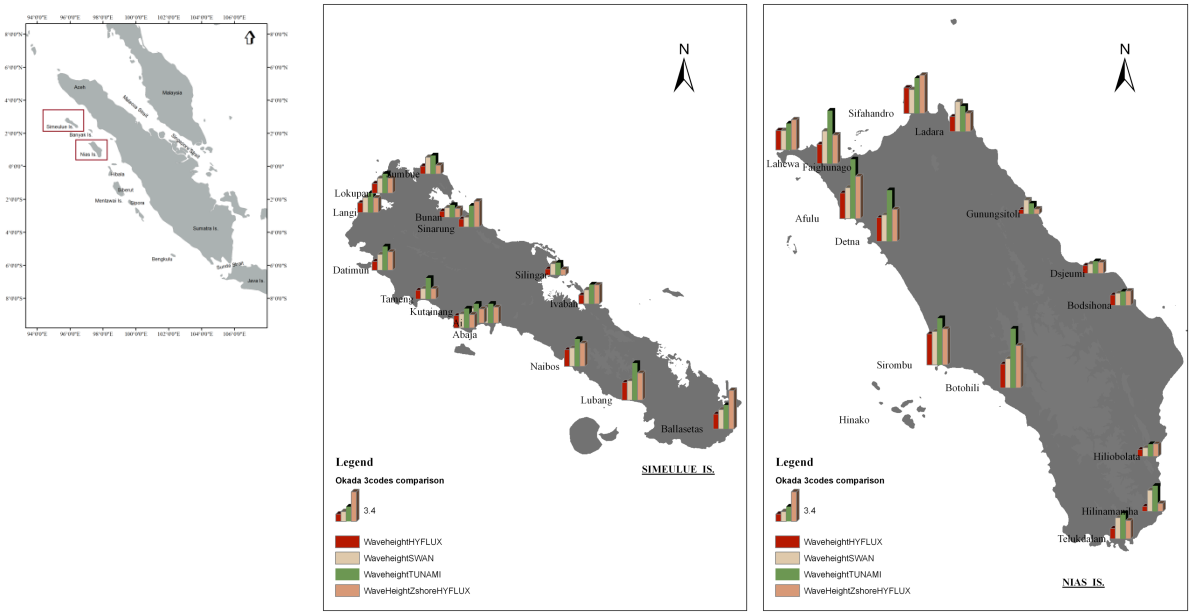

Figure 3.7. Comparison of simulated wave heights using different numerical codes using gCMT model. Grid size used in simulations is 900 m.

Wave height and inundation distance values are shown in figure 3.8. It could be seen that sites such as NW Nias are overstimated wave height zmaxShore is 3.42 m and measured wave height at this location is 0.5 m. Similarly at Banyaks, measurements are smaller than the simulated wave heights. On the contrary for Sibolga and along Sumatra coast wave height values are very similar (Fig. 3.8). These results confirm the importance to evaluate near field tsunamis, mainly for regions like western Indonesia with islands along main rupture area.

Finally, comparisons of the horizontal inundations measures with the simulations cannot be done because the maximum inundation extend is in the same order of magnitude of the grid size: the ratio between the horizontal inundation and the grid size should be at least 10, i.e. in order to capture an inundation of 300 m the grid size should be lower than 30 m (Franchello and Annunziato, 2012).

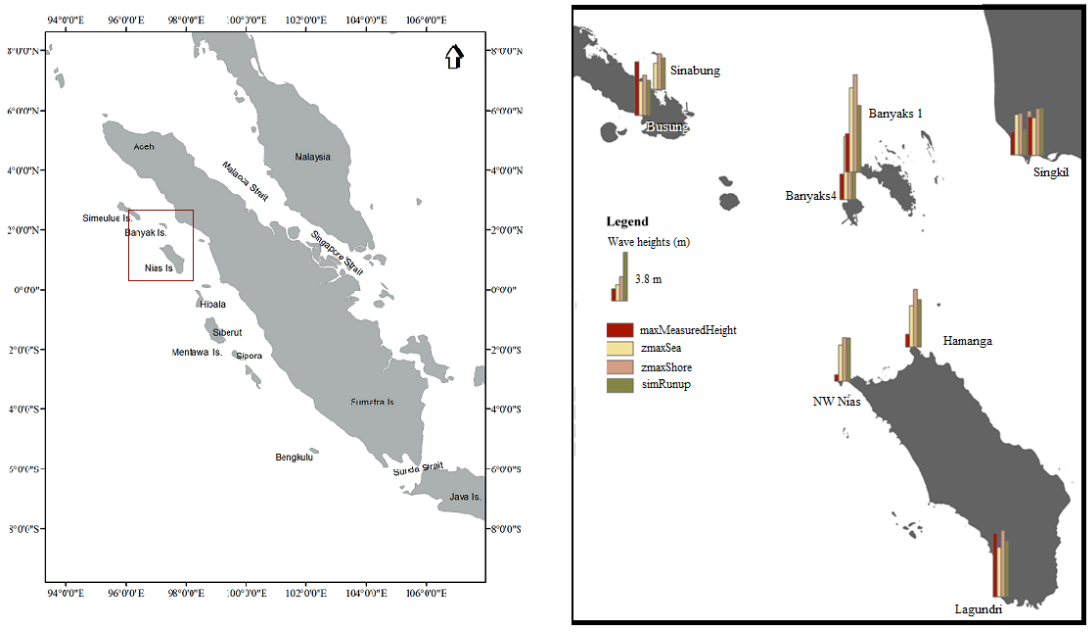

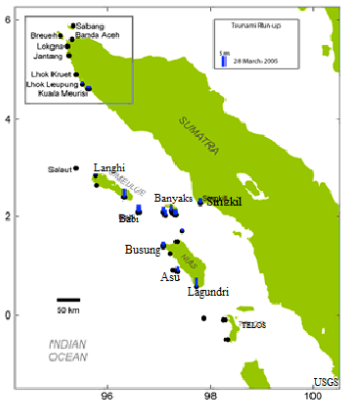

Site	Latitude	Longitude	maxMeasuredHeight	zmaxSea	zmaxShore	simulatedRunup
Sibolga	1.73	98.79	1.20	1.030	1.305	
Singkil	2.27	97.78	1.00	2.072	3.504	1.78
Langhi	2.82	95.74	0.50	1.630	1.723	
Busung	2.42	96.32	4.20	2.692	3.146	0.75
Babi	2.08	96.62	2.00	2.862	3.153	
Banyaks1	2.1	97.10	2.00	4.949	4.852	2.96
Banyaks4	2.05	97.10	2.00	3.854	4.519	
Singkil2	2.27	97.75	1.80	3.174	3.253	1.93
NW Nias	1.41	97.08	0.50	2.836	3.412	3.38
Lagundri	0.59	97.68	5.00	3.895	5.223	4.41
Asu	0.82	97.35	2.50	2.668	2.723	
Kariya Vhapi	2.83	95.74	3.20	1.557	1.709	
Sinabang	2.52	96.38	0.00	2.047	2.802	2.47
Port of Singkil	2.27	97.82	3.00	2.947	3.665	3.73
Hamanga beach	1.54	97.35	1.00	3.241	4.513	3.72
Lagundri Bay	0.57	97.75	4.00	2.363	3.042	

Figure 3.8. Selected points to show results of 900 m calculation. Simulated (sim) and measured (mes) values are shown. Water height and distances shown in meters.

3.4 Inundation assessment using HyFlux2

Within inundation assessment procedure many limitations are faced, mainly related to numerical scheme and bathymetry resolution. We have performed here simulations with available 300 m resolution. For more detailed bathymetry HyFlux2 code use resulting boundary conditions of previous coarser simulations.

Tsunami wave parameters close to the shoreline and inland can be measured with tidal gauges and with information acquired from field surveys after the event (USGS, 2005a). Tsunami evidence of the 2005 Nias tsunami was found along 500 km of the Indonesian coast. In this region the maximum run-up elevations were approximately 4 meters (USGS, 2005a).

We are aware that caution is needed when measured data is compared since the resolutions used for in this project are in the range of medium resolution. Thus one cannot expect to use this survey so punctual. However, it is important to use field data to have an idea of the bias of simulation results compared to what was measured on the field and using available bathymetry.

3.4.1 Singkil, Sumatra Island: grid 1

At Singkil-Baru site, NOAA-NGDC reported subsidence and 1 m water height. According to local reports, tsunami arrived 10 to 15 minutes after the earthquake and came as one large surge that stayed for almost an hour. Field watermark elevations were reported in the range of 1.5 to 1.8 m above the present sea level. The tsunami inundated approximately 200 m inland from the pre-earthquake shoreline (USGS, 2005a). Maximum simulated water height at Bankoengan is 2.15 m and 3.8 m at the Pasar Singkil. Simulation show good agreement with measured run-up (Fig. 3.9). The following chart (Table 1) shows the parameters used in the nested simulations.

Table 1. Parameters of simulation summarized.

Focal mechanism	Strike: 329°	Dip: 8°	Rake: 109 °	Slip: 6.4 m
Okada Model	Maximum coseismic uplift:			
Grid 1: 180 m resolution	Lon max: 98°	Lon min: 97°	Lat max: 3°	Lat min: 2°
Grid 2: 180 m resolution	Lon max: 96.5°	Lon min: 95.5°	Lat max: 3°	Lat min: 2°
Grid 3: 180 m resolution	Lon max: 98°	Lon min: 97°	Lat max: 1.5°	Lat min: 0.4°

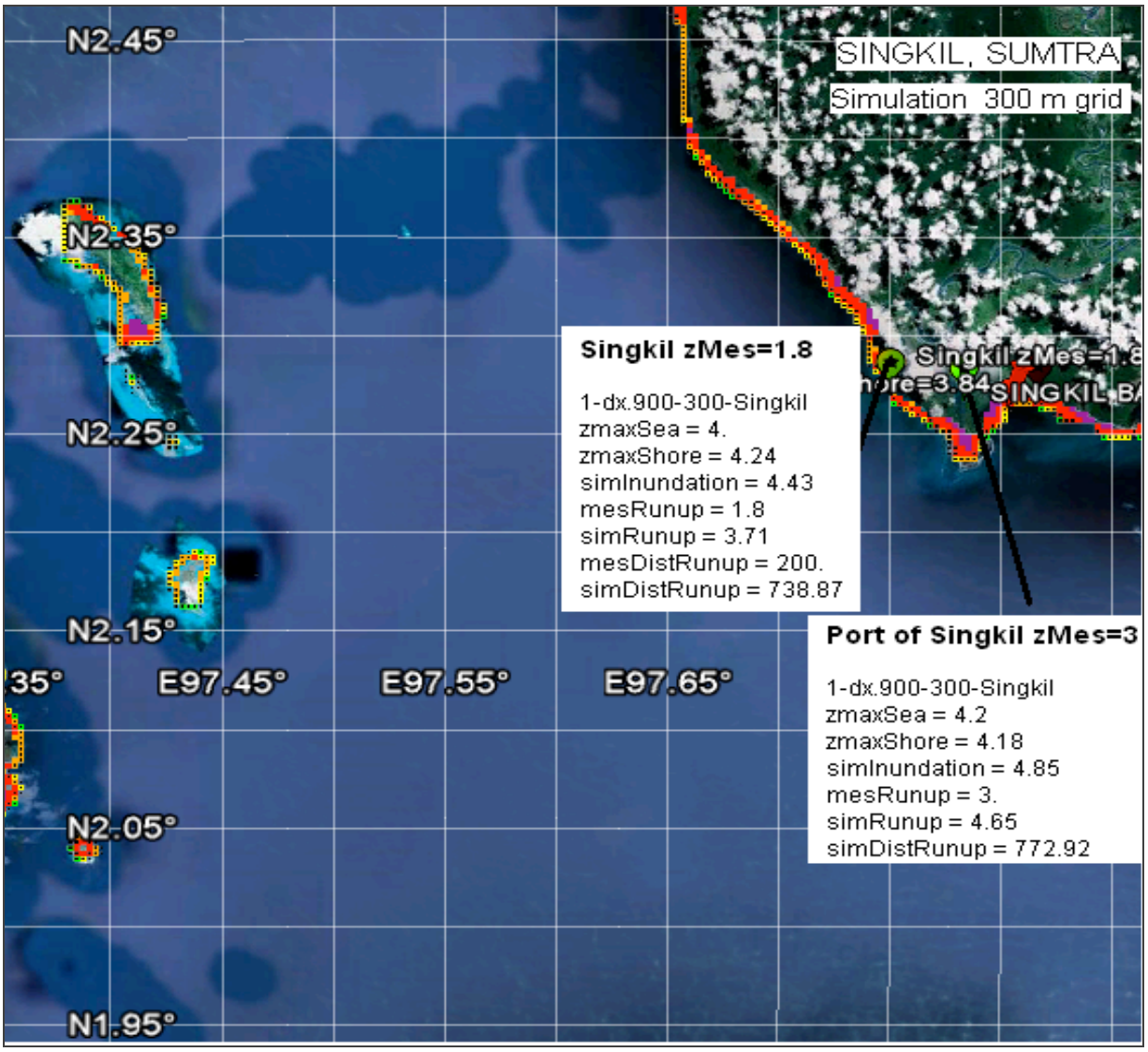

Figure 3.9. Sites in Sumatra Island where calculations could be compared with field measurements.

3.4.2 Simeulue Island: grid 2

The fishing village of Kariya Vhapi on the NW shore of Simuelue, was affected by a flow higher than 3.2 m that overtopped a high berm (USGS, 2005). At the shoreline subestimated wave heights of 1-1.5 m were simulated. The 28 March tsunami was large at Gusong Bay, Busung **(**SW Simeulue Island**)**. The team measured tsunami run-up of 4.2 m and the simulated run-up is 3.08 m, whereas at run-up is overestimated in simulation.

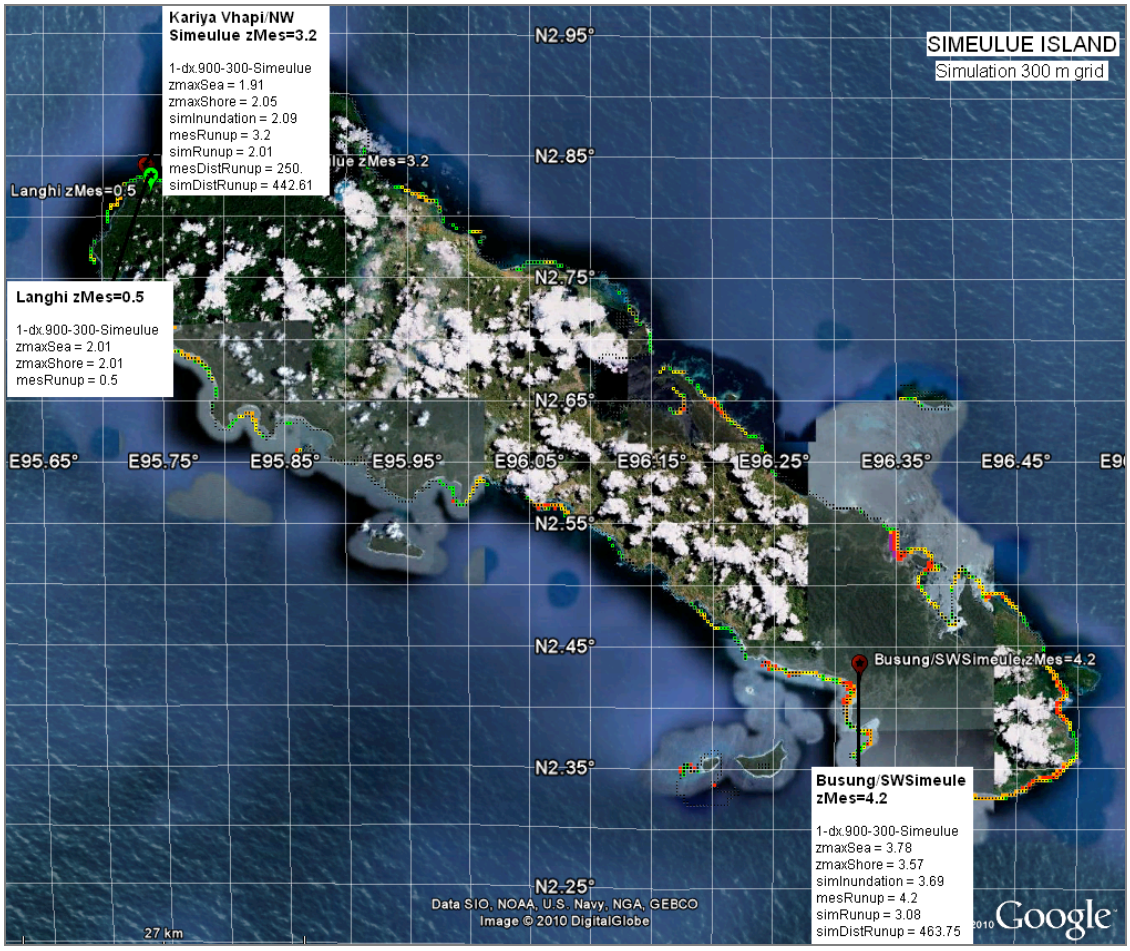

Figure 3.10 Three sites where calculations could be compared with field measurements. Ratio 0.68 (simRun-up/mesRun-up).

34.3 Nias Island: grid 3

Nias Island sites were very affected by the tsunami according to field measurements (USGS, 2005a*)*. The Nias tsunami was larger than the 26 December tsunami at Lagundri Bay in SW Nias Island. At the specific site of Lagundri Bay, SW Nias Island tsunami run-up of 3 to 4 m and inundation distances of 400 to 500 m were measured. Uplift was small here, less than 0.3 m. The tsunami arrived 5 to 15 minutes after the earthquake on 28 March. The simulated distance of 379 m is close to the 400-500 m measured for this site (Fig. 3.11; 3.12). Considering that the measured distance is in the same order of the grid size, the simulation results should be considered only qualitatively: however, the simulated maximum water height in the shoreline and the maximum run-up distance are information that can be used for early identification of the run-up areas, without to pretend to estimate in detail the amount of the inundated area.

The 28 March 2005 earthquake cause uplift in the island of Asu 1 to 2 meters, exposing coral reef. Simulated wave height offshore is 4.43 but no run-up, this could be related to high uplifted on the area.

As a final point, in order to have a reliable sea level prediction on the coast it is however necessary to use much finer nodalizations. We have used 300 m resolution grid to calculate also the inundation phase. However results of Samoa tsunami assessment using HyFlux2 where detailed bathymetry of 10 m was available showed even better performance (Franchello and Annunziato, 2012). Update Nias 2005 tsunami evaluation using new seismological and remote sensing data will be very valuable also when more fine bathymetry and topography are available.

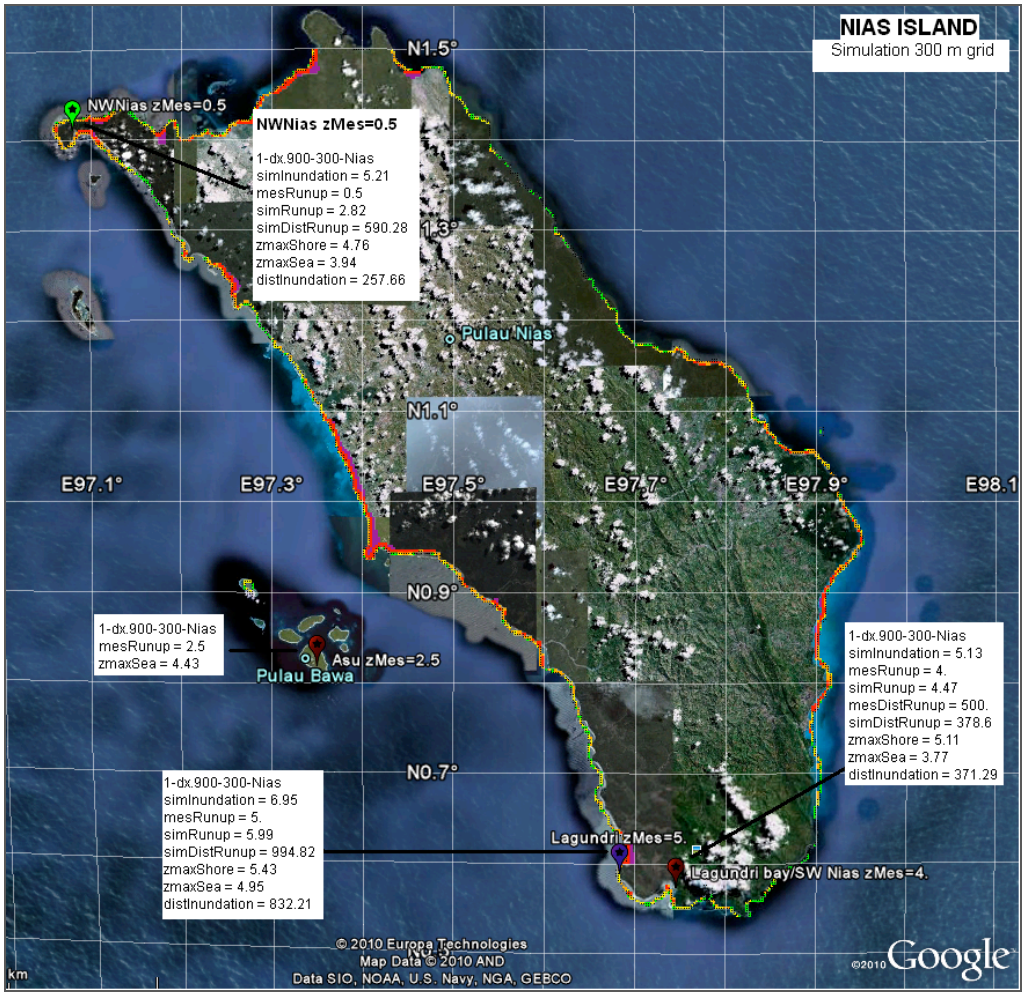

Figure 3.11. Sites where calculations could be compared with field measurements.

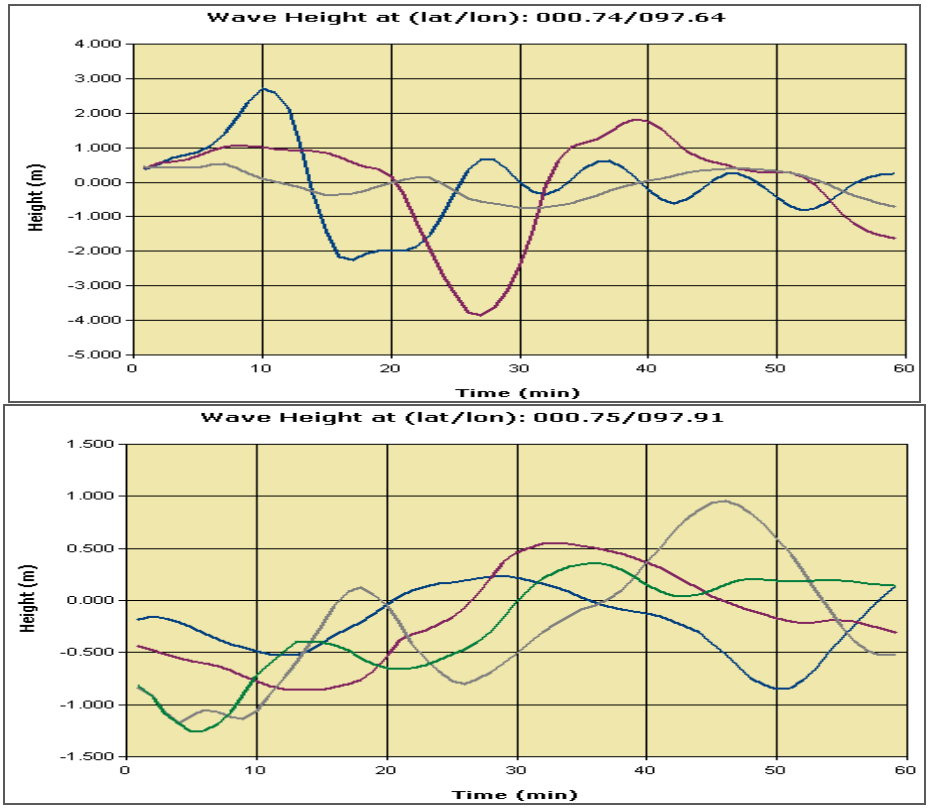

Figure 3.12. a. Sea level at south Nias: sensor S5(blue), S6 (pink) and S7 (grey). b. Sea level at S-SE Nias: sensor S8(blue), S9 (pink), S10 (grey) and S11 (green).

4. CONCLUSIONS

The tsunami analysis depends strongly on: a) the initial fault mechanism; b) the hydraulic conditions (e.g. bathymetry cell size). It is also important to point out that the information available immediately after the events are only epicenter, magnitude and depth. All these quantities may change significantly due to progressive improvement of the seismological parameters provided by the seismological centers. In addition grid resolution is very important, for example medium resolution simulations of 300 m give different results when comparing with the high resolution (5 minutes, 1 minute) as it is expected. In addition the ideal for assessing wave inundation is to have bathymetry resolution at least finer than 30 m. However, wave height trends, mainly the first wave simulated with coarser resolutions do not show great differences except when we compare the three main numerical codes under study.

Propagation results have been very reliable and consistent for the assessed codes; while for the inundation limitation still exist. In order to have a reliable sea level prediction on the coast it is

however necessary to use much finer nodalizations. This was done by using a 300 m resolution grid and the HyFlux2 code was used to calculate also the inundation phase. Considering that the measured distance were in the same order of the grid size, the simulation results can be considered qualitatively, allowing an early identification of the run-up areas, without to intend to estimate in detail the amount of the inundated area. Better bathymetry resolution could have even improved the results but it was not available. In other reports it was shown that 30 m resolution could has noticeably improved the local response.

HyFlux2 code show smoother results in the sea level trends than TUNAMI-N2 and JRC-SWAN code. In simulated wave heights resulted at the shoreline the HyFlux2 code shows less oscillations in respect to the other codes, explaining why the maximum water surface level were under estimated in respect to the other codes. HyFlux2 numerical approach makes robust performance and reliability for inundation assessment

As evaluated along Banyaks and Nias Islands where high deformation was measured on the field was not represented in fault models. Nias 2005 event was an interesting case to evaluate crustal deformation and how this deformation is being reproduced by the fault models to get the initial water column displacement. Thus, cases like 2005 Sumatra, among others, have been good cases to evaluate this approach. We can conclude that still a challenge for early warning systems to get the most reliable fault mechanism minutes after the earthquake.

ACKNOWLEDGEMENT

We acknowledge Dr. Gegar S. Prasetya for advices given at the beginning of this research. We thank Dr. Gavin Hayes (USGS) for providing Finite Fault Model of Northern Sumatra (Nias) earthquake. Figure 1 has been done using GMT 4.5.8. N.Z Acknowledge EC-JRC for training program in tsunami modelling.

REFERENCES

Annunziato, A. (2005). Development and Implementation of a Tsunami Wave Propagation Model at JRC. **Proceedings of the International Symposium on Ocean Wave Measurement and Analysis**. Fifth International Symposium on Ocean Wave Measurement and Analysis. Madrid 3-7.

Annunziato, A. (2007). The Tsunami Assessment Modelling System by the Joint Research Centre. *Science of Tsunami Hazards* **26:2**, 70-92.

Briggs, R.W. (2006). Deformation and slip along the Sunda megathrust in the great 2005 Nias–Simeulue earthquake. *Science* 311, 1897-1901.

Castro, C.E., Toro, E.F. and Käser, M. (2012). ADER scheme on unstructured meshes for shallow water: simulation of tsunami waves. *Geophys. J. Int.* **189:3**, 1505-1520.

Falck, C., Ramatschi, M., Subarya, C., Bartsch, M., Merx, A., Hoeberechts, J., and Schmid, G. (2010). Near real-time GPS applications for tsunami early warning systems. *Nat. Hazards Earth Syst. Sci.* **10**, 181-189.

Franchello, G. (2008). Modelling shallow water flows by a High Resolution Riemann Solver. JRC Scientific and Technical Reports. **EUR 23307** EN 34p.

Franchello, G. (2010). Shoreline tracking and implicit source terms for a well balanced inundation model. *International Journal for Numerical Methods in Fluids* **63:10**, 1123-1146.

Franchello, G. and Annunziato, A. (2012). The Samoa tsunami of 29 September 2009- Early Warning System and Inundation Assessment. *Science of Tsunami Hazards* **31:1**, 19-612.

Geist, E. L., and Dmowska, R. (1999). Local tsunamis and distributed slip at the source. Pure and Appl. Geophys. **154**, 485-512.

Geist, E., Bilek, S.L., Arcas, D. and Titov, V.V. (2006). Differences in tsunami generation between the December 26, 2004 and March 28, 2005 Sumatra earthquakes. *Earth Planets Space* **58,** 185-193.

Geist, E., Titov, V.V., Arcas, D. Pollitz, F.P. and Bilek, S.L. (2007). Implications of the December 26, 2004 Sumatra-Andaman earthquake on tsunami forecast and assessment models for great subduction zone earthquakes. *Bull. Seis. Soc. .Amer*. **97, 1A,** S249-S270.

Goto, C., Ogawa, Y., Shuto, N. and Imamura, F. (1997). Numerical Method of Tsunami Simulation with the Leap-Frog Scheme. IUGG/IOC TIME Project Intergovernmental Oceanographic Commission of UNESCO. *Manuals and Guides* **36:26**, 126 p.

Imamura, F. (1996). Simulation of wave-packet propagation along sloping beach by TUNAMI-code: Long-wave Run-up Models edited by H.Yeh, P.Liu and C.Synolakis. World Scientific I981, 231-241 p.

Imamura, F., Yalciner, A.C. and Ozyurt, G. (2006). Tsunami Modeling manual - TUNAMI-N2 (Tohoku University's Numerical Analysis Model for Investigation of Near Field Tsunamis ver. 2) http://www.tsunami.civil.tohoku.ac.jp/hokusai3/J/projects/manual-ver-3.1.pdf. (Accessed 02/15/2010).

Ji, C., Wald, D.J. and Helmberger, D.V. (2002). Source description of the 1999 Hector Mine, California earthquake; Part I: Wavelet domain inversion theory and resolution analysis. *Bull. Seis. Soc. Am*er. **92:4**, 1192-1207.

Liu, P., Yeh, H., Lin, P., Chang, K.T. and Cho, Y.S. (1998). Generation and evolution of edge-wave packets, Phys. Fluids **10**: 7, 1635-1657.

Mader, C.L. (1974). Numerical Simulation of Tsunamis. *J. Phy. Ocean.* **4:** 74.

Mader, C.L. (1988). Numerical modeling of water waves. University of California Press, Berkeley, California.

Mader, C.L. (2004). Numerical Modeling of Water Waves. 2nd ed., CRC Press, Boca Raton, Fl. 274p.

McCaffrey, R. (2009). The Tectonic Framework of the Sumatran Subduction Zone. Annu. *Rev. Earth. Planet. Sci.* **37**, 345-366.

NOAA, National Oceanic and Atmospheric Administration website: http://nctr.pmel.noaa.gov/tda_documentation.html. (Accesed 11/15/2010).

Okada, Y. (1985). Surface deformation due to shear and tensile faults in a half-space. Bull. of the Seis. Soc. of Amer. **75**,1135–1154.

Prawirodirdjo, L. and Bock, Y. (2004), Instantaneous global plate motion model from 12 years of continuous GPS observations, *J. Geophys. Res.* **109**, B08405.

Sobolev, S.V, Babeyko, A., Wang, R., Galas, R., Rothacher, M., Sein, D.V., Schröter, J., Lauterjung, J. andSubarya, C. (2007). Concept for fast and reliable tsunami early warning using "GPS-Shield" arrays. *J. Geophys. Res*. **112**, B08415.

Song, Y.T. (2007). Detecting tsunami genesis and scales directly from coastal GPS stations. *Geophys Res. Lett.*, **34,** L19602.

Subarya, C., Chlieh, M., Prawirodirdjo, L., Avouac, J.P., Bock, Y., Sieh, K., Meltzner, A.J., Natawidjaja, D.H. and McCaffrey, R. (2006). Plate-boundary deformation associated with the great Sumatra–Andaman earthquake. *Nature* **440**, 46-51.

Titov, V.V., Gonzalez, F., Bernard, E.N., Eble, M.C., Mofjeld, H., Newman, J.C and Venturato, A.J. (2005). Real-Time Tsunami Forecasting: Challenges and Solutions. *Natural Hazards* **35**, 41–58.

USC - http://earth.usc.edu/~jrdonova/finite_fault_links.html

USGS, 2005a - http://walrus.wr.usgs.gov/news/reports.html. (Accesed 12/06/2012).

USGS, 2005b - http://earthquake.usgs.gov/regional/neic. (Accesed 12/06/2012).

Ward, S .N. (2002). Tsunamis. Encyclopedia of Physical Science and Technology. Ed. Meyers, R.A., Academic Press, **VOL XVII**: 175–191.

Zamora-Sauma, N., Franchello, G. and Annunziato, A. (2011). 1 April 2007 Solomon Island tsunami: case study to validate JRC tsunami codes. Joint Research Centre – Institute for the Protection and Security of the Citizen. **EUR 24783** EN, 63p.

ISSN 8755-6839

SCIENCE OF **TSUNAMI HAZARDS**

Journal of Tsunami Society International

Volume 33 **Number 2** **2014**

IMPROVING EXPERIMENT DESIGN SKILLS: USING THE JOKO TINGKIR PROGRAM AS A LEARNING TOOL OF TSUNAMI TOPIC

Madlazim and Supriyono

Physics Department, Faculty of Mathematics and Science, Universitas Negeri Surabaya (UNESA), INDONESIA
e-mail: madlazim@fmipa.unesa.ac.id

ABSTRACT

Students are rarely given an opportunity to think deeply about experimental design or asked to develop experimental skills on their own. Without participating in these endeavors, they are often unaware of the many decisions necessary to construct a precise methodology. This article describes the Joko Tingkir Program as an Early Warning Tsunami, and how we have used this program as a learning tool for physics teacher candidates to improve their experimental design skills. The Joko Tingkir computer program has implemented a Tsunami Faulting Model (TFM). The TFM uses the principle that the tsunami is affected by the length and width of earthquake rupture. Both can be represented by the duration of rupture (Tdur) or Exceed 50 second duration (T50Ex) and the dominant period (Td). The TFM has been implemented by the Joko Tingkir computer program. When students are given a simple method using the Joko Tingkir program - such as the tutorial, observation of seismic station distribution, seismograms of the earthquake, equipment and software for this experiment, measurement of P time onset and determination of Tdur, Td and T50Ex - it allows them to focus exclusively on improving experiment design skills as indicated by significantly improved gain scores. Based on the gain analysis it can be inferred that the experiment design skills can be improved by implementation of Joko Tingkir Program as a Learning Tool of Tsunami Warning in the learning process

Key word: *Experiment design skills, rupture duration, exceed duration 50 second, dominant period, Joko Tingkir program.*

Vol. 33, No. 2, page 133 (2014)

1. INTRODUCTION

Scientific inquiry is fundamental in conducting experimental science. Exposing undergraduate students to this process of inquiry can be challenging, especially when teaching courses that do not have an associated laboratory section. Many students are not familiar with how to develop a testable hypothesis or they may believe that they do not know enough about scientific methods to design an experiment. Indeed, student misconceptions and inaccuracies regarding randomization, sample size, and proper controls have been described at the college-level (Anderson-Cook and Dorai-Raj, 2001; Hiebert, 2007), at the graduate-level (Zolman, 1999), as well as in professional publishing in life sciences (Festing, 2003). However, by using a simple experimental measure, students can become engaged in the process of scientific inquiry and, in turn begin to think deeply about experimental design. As an example of the power of this approach, this paper describes how we have used the Joko Tingkir program for physics teacher candidates as a means to have them improve issues related to experimental design.

For pedagogical purposes, Etkina et al (2006) have classified experimental investigations that students perform in introductory courses into three broad categories: observational experiments, testing experiments and application experiments. When conducting an observational experiment, a student focuses on investigating a physical phenomenon without having expectations of its outcomes. When conducting a testing experiment, a student has an expectation of its outcome based on concepts constructed from prior experiences. In an application experiment, a student uses established concepts or relationships to address practical problems. In the process of scientific research the same experiment can fall into more than one of these categories. Etkina et al (2006) have identified the following steps that students need to take to design, execute and make sense out of a particular experimental investigation.

Some methods and applications are available and have been proposed and has been applied to determine the source parameters of earthquakes for a tsunami early warning system. Along with other parameters, seismic moment magnitude (*M*w) is found to be a good discriminant for many, past, tsunamigenic earthquakes but not for all them – particularly for the so-called 'tsunami earthquakes' which, by definition, cause larger tsunami waves than would be expected from calculated moment magnitudes, *M*w (e.g. Satake, 2002; Polet & Kanamori, 2009; Lomax & Michelini, 2011). The discrepancy for these earthquakes can be related to rupture at shallow depth where the parameter designated as "μ" can be a very low, anelastic deformation occurring by compression and uplift of sediments, or when the fault surface may be non-planar with splay faulting into the accretionary wedge (e.g. Lay & Bilek 2007) and as postulated for the great 2011 Tohoku-Oki tsunamigenic event Pararas-Carayannis (2013). One or more of these effects can result in an underestimate by *M*w of an effective *LWD* value by a factor of four or more, relative to the value needed to explain the observed tsunami waves (Okal 1988; Satake 1994; Geist & Bilek 2001; Lay & Bilek 2007; Polet & Kanamori 2009; Lomax & Michelini, 2011).

Several analyses of teleseismic, *P*-wave seismograms (30◦–90◦ great-circle distance; GCD), (Lomax & Michelini, 2009) have shown that a high frequency, apparent rupture-duration, "*T*0", greater than about 50 seconds forms a reliable discriminant for tsunamigenic earthquakes (Fig. 1). Lomax & Michelini (2009) exploit this result through a direct, duration-exceedance (DE) procedure applied to seismograms at 10°–30° GCD, to rapidly determine if the rupture duration "*T*0" of an earthquake is likely to exceed 50–55 seconds and thus be potentially tsunamigenic, and based on the analysis of seismic parameters Madlazim (2013) and with the present study, help explain why one earthquake event generates a tsunami, while another one does not.

In this study, we present improved experimental design skills by using the Joko Tingkir program as a Learning Tool of Tsunami Faulting Model (TFM) and by implementing a direct procedure for assessing potential tsunami generation (Lomax & Michelini, 2009; 2011; 2012, Madlazim, 2011; 2012; 2013). The method is based on combining rupture duration (Tdur) with a measure of the dominant period (Td) and a duration exceedance 50 seconds (T50Ex) as determined simultaneously by local velocity records of stations of the real-time early, tsunami warning system. Tdur, *T*d and *T50Ex* are simple to measure on observed, *P*-wave seismograms and can be related to the critical parameters rupture of length (*L*), width (*W*), slip (*D*) and depth, such parameters needed for assessing tsunami generation potential (Lomax and Michelini, 2011).

2. THE JOKO TINGKIR PROGRAM

Briefly, Joko Tingkir is a script program which calculates three parameters as indicators of a potentially tsunamigenic earthquake. These parameters are Tdur (Rupture duration), Td (Dominant Period), T50Ex, and the Products (Tdur*Td, T50Ex*Td), simultaneously. Tdur is associate/equivalent with the length of the rupture zone, Td is associated/equivalent with the width of the rupture zone and T50Ex is associate/equivalent with the length of the rupture zone (a better estimate than Tdur). The products are related with the area of the rupture zone and the Strength Scale of the earthquake source.

The Joko Tingkir Program can directly read the data from seismograms in mini-seed format by using the SeisGram2K software (http://alomax.free.fr/software.html), which is faster than reading seismograms in real time, without the need to first convert into other formats or SAC. The computational speed of determining the earthquake parameters is dependent on the amount of data processed. For example, if the amount of data that is being processed is related to the vertical components of 20 recorded seismograms by 20 stations, and then the time required by the Joko Tingkir Program to compute these parameters is approximately 18 seconds.

The output of the Joko Tingkir Program - in addition to mean values of Tdur, Td, T50Ex, Td * T50Ex - also provides values of Tdur, Td and T50Ex for each station, so that the user can evaluate whether Tdur, Td and T50Ex at each of the stations is valid and homogeneous when compared with the value Tdur, Td and T50Ex on most other stations. If the value Tdur, Td, T50Ex and Td * T50Ex are more than a critical value, then it can be implied that an earthquake is potentially tsunamigenic. Thus, by using the Joko Tingkir Program, an early tsunami warning could be announced in less than 5 minutes after earthquake occurrence, so that the public and the relevant civil defense agencies will

have more time to prepare for evacuation of the coastal areas at risk. The last step is the plotting of the Joko Tingkir Program results, particularly the Tdur, Td, T50Ex, T50Ex*Td and Tdur*Td solutions and the decision making on whether a tsunami was generated or not can be obtained about 4 minutes after the earthquake occurrence (Fig. 1).

2a. The Joko Tingkir Program as a Learning Tool In Improving Experiment Design Skills

We used the above-described Joko Tingkir program as a Learning Tool for improving students' experimental design skills by enabling them to measure an earthquake's length of rupture and in developing a strategy to incorporate the findings into an experimental design. To accomplish this goal we implemented the Four Question Strategy (FQS), as described in the literature (Cothron et al, 1989; Science Pioneer), by applying it to the tsunami-warning problem. With this method, we can have the students explore the possible variations of a research topic before attempting to state a problem, write a hypothesis, and identify variable, constants and in setting control parameters. Students need a method that is tried and proven and then practice it to measure tsunami parameters several times before designing an original experiment of their own. The FQS is a skill that is guaranteed to strengthen with practice but is not likely to be mastered in any one session. Students can even apply the approach, but must be given simple materials with few variations

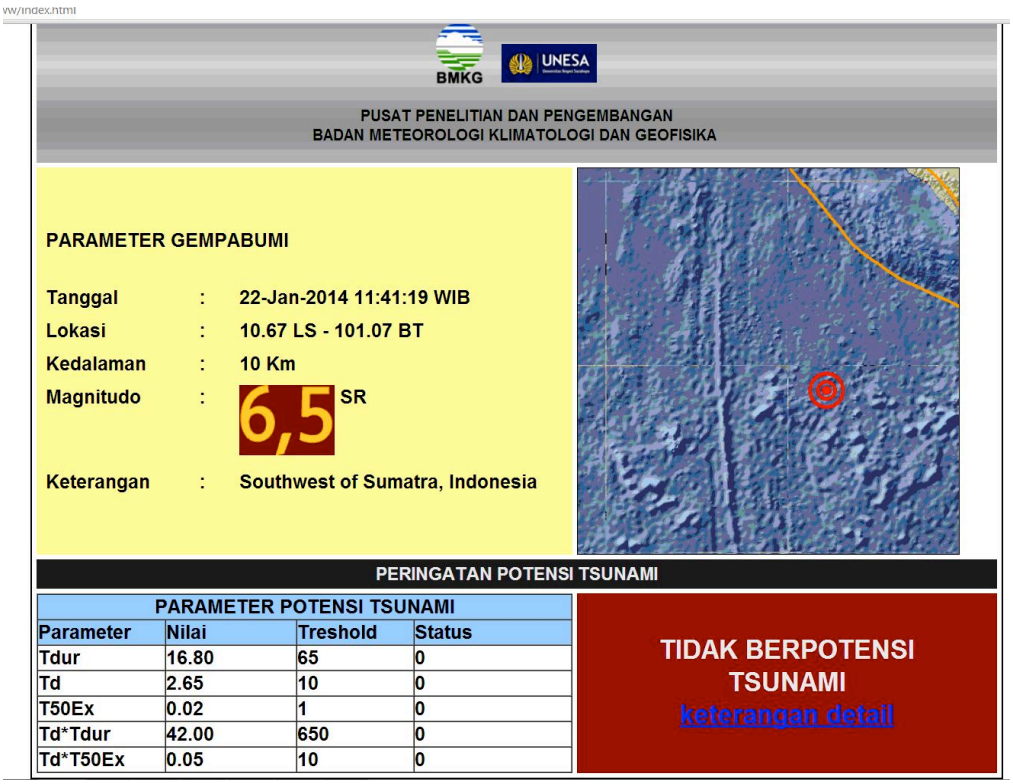

Figure 1. The Joko Tingkir real time system plotting result (Madlazim et al, 2014; Masturyono et al.; 2013).

.

The use and implementation of the FQS learning process requires four steps (Cothron et al, 19890:

Step one - the relevant question is: What materials are readily available for conducting experiments on the earthquake topic (e.g. tsunami) and then listing them in writing.

Step two - requires asking the question: How does an earthquake relate to a tsunami? One response is: an earthquake can generate A Tsunami. This step is the most difficult because children typically think actions are behaviors and in a sense, here we can say, "How does a tsunami behave?" However, with other physical or earth science topics, it may be more difficult to identify how relevant is a resulting disaster. For example, "How does a tsunami impact a coastline?" The point of this question is to focus on what tsunami actions/effects can be measured.

Step Three - In *Step Three* the question to be answered is: How can one measure, describe or evaluate the potential action of the tsunami or of the needed response? Some responses may include: *Measure the length of the longest earthquake rupture.* If students had difficulty with *Step Two*, going on to *Step Three* may make *Step Two* easier to understand. This is the data collection phase of experimental design. An important part of the question is: What can you measure? Linear measurement comes quickly to students. However, counting objects, frequency, time, volume, mass, etc. are other measurement options that might be more appropriate than linear measurements in an experiment. Another important point is that an experiment is not always contingent on actual measurements. Written descriptions are very acceptable. If a written description is the method of data collection, then time must be spent in teaching the students to be precise about the words they use. This part of the experiment is call the Dependent Variable, or how you can document change.

Step four - is the final step where brainstorming and creativity begin to evolve. It is here that students will identify the variables they will be testing in the experiment. Each tested variable becomes a different experiment. *Step Four* may be introduced by going back to *Step One*, which was to identify the materials needed to experiment with the topic. The question that needs to be answered is: How can you change the set of tsunami topic materials to affect the action or the impact behavior? It must be remembered that it is the action or the impact/behavior, which needs to be measured. At this point one must refer to the list of materials in *Step One*. If these are listed in a vertical column, they need to be placed as horizontal "column headlines". Exploring one material item at a time (i.e. length of rupture) - rather than skipping around - is better because the students remain focused.

After the students have exhausted the way they could vary this item, then they must move on to the next variable. The variable that will be deliberately changed or altered becomes the Independent Variable. All other listed variables (materials) must remain constant, because if more than one is altered; it will be too difficult to know which caused the change. As students increase their skills and sophistication, they can alter more than one variable or study different correlations. The control is the "set-up" that is not affected by the independent variable. It will not receive the same treatment. This set-up is the one that the others will be compared to. Having completed these tasks, the students are now ready to write their experimental question, purpose and hypothesis. The question contains two items: material (variable in *Step Four*) and how the change will be measured (*Step Three*). For example, if the independent variable is the length of earthquake rupture and the dependent variable is

how the change in tsunami generation will be measured, the resulting question is: *Does the length ofrupture* affect *tsunami generation*? The hypothesis can simply answer the question: Indeed, the length of rupture affects tsunami generation. In the scientific method, the purpose is an expansion of the explanation (more explanation) of the hypothesis. What does one want to find out or what knowledge does one want to support? The procedure should be a sequence of steps the student will follow to find the answer to the question in order of fulfilling the purpose of his/her inquiry. Data collection strategies must be included in this part. Students must be discouraged from using transitional words for sequence. Having the students write the steps in sequence and by beginning each step with a verb will help them make the directions become more precise and clear. The material is a thorough list of items needed to complete the experiment. Thus, students must be encouraged to be very specific. The results must include data displays (i.e. charts, graphs, tables), and an explanation of what the data represents. It is also a good opportunity to have the students take notes that might explain along the way the effect of the outcomes. The final conclusion is an explanation of why the student researcher thinks he or she arrived at their results. This is the point when the researcher is better prepared to do further research on the question. In conclusion, the student should reflect on why the data did or did not support the hypothesis. This is also a good place to suggest the next steps the researcher might take to further explore the topic.

As stated earlier, further sessions in designing experiments are a skill that needs to be introduced in a simple manner and practiced frequently. The instructor may want to spend a session on one step at a time but if the students are familiar with the experimental design, one session of the four-step strategy may be enough to get them going. For a follow-up session, students as a group may be given a topic, which may be run through the described steps in order to reach a research question and a hypothesis.

3. METHOD

Students' performance was assessed by the administration of a diagnostic test for experiment design skills on the first and last day of control and experiment class; only students who took both pre-test and post-tests are part of the sample. The diagnostic instrument was the experiment design skills. This is the 13-item Liker-scale related to experiment design ability evaluation. The experiment design skills evaluation is almost entirely on a qualitative scale. The evaluation was adapted from Karelina and Etkina(2007) and Science Pioneers

(http://www.sciencepioneers.org/sites/default/files/documents/ Experimental Design vs ScientificMethod_0.pdf)
and modified to measure the students' performance. The test contained thirteen indicators with a maximum score of 52. The instrument was given for validation to four experts in physics education. The reliability of test was ascertained by control-testing it using a class of physics education students at Universitas Negeri Surabaya, Indonesia, which was not been included in the study but had similar characteristics as the sample classes. The reliability coefficient was calculated using that described in Kolen et al. (1996). This method is suitable when a performance scale can be scored. The reliability coefficient of the performance assessments instrument was 0.84 which rounds of to α=0.76.

According to Fraenkel and Wallen (2000), an alpha value of 0.7 and above is considered suitable to make group inferences that are accurate enough. On the pretest, students were given enough time to demonstrate their experiment design skills on a format that consisted of the 13 indicators. On the last day of class, the same evaluation was administered as a pos-test to assess experiment design skills after training by use of Joko Tingkir, as a Tsunami Warning Program treatment for both the control and the experiment class. The content used in class instruction was developed based on the revised 2011/2012 physics syllabus of the Physics Department, Mathematics and Science Faculty, of UNESA. A guiding manual was compiled for the lecturers in administering learning using Joko Tingkir as a Tsunami Warning Program for the purpose of improving the student's experiment design, used throughout the treatment period.

4. RESULTS AND DISCUSSION

The results of the pre-test scores on experiment design skills evaluation for both control and experiment classes showed statistically with significance 0.746 and > 0,05, respectively. The difference between the samples is regarded as not significant. This indicated that the two classes used in the study exhibited comparable characteristics as shown by Table 1 and Table 2. Therefore, the classes were suitable for the conduct of the study when comparing the results of learning using the Joko Tingkir Program as a learning Tool of Tsunami Warning and as a regular learning method on experiment design skills.

Table 1. Result of the Mann-Whitney Test

Ranks

	Class	N	Mean Rank	Sum of Ranks
pretest	Experiment Class	40	41,34	1653,50
	Traditional Class	40	39,66	1586,50
	Total	80		

Table 2. Result of the Mann-Whitney Test

Test Statistics[a]

	pretest
Mann-Whitney U	766,500
Wilcoxon W	1586,500
Z	-,324
Asymp. Sig. (2-tailed)	,746

Figure 2 shows that the average gain (gr) is smaller than the student individual gain (g) and that the students with low pre-test scores tend to have larger score improvements than the students of the experiment class, with high pretest scores. While the control class shows that the average gain (gr) is the greater than student individual gain (g), students with low pre-test scores tend to have

either smaller or similar score improvement than students with high pre-test scores. Bao (2006) interpreted that he made inferences about how the experiment class of students has changed. For the traditional class, gr is greater than g; so that we can infer that students with low pre-test scores tend to have either smaller or similar score improvement than students with high pre-test scores. For the Joko Tingkir Program with FQS class, gr is smaller than g, so that students with low pre-test scores tend to have larger score improvements than students with high pretest scores.

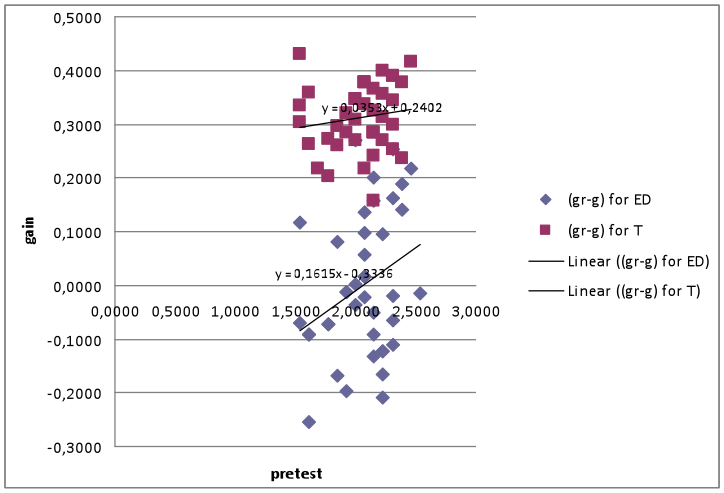

Figure 2. Y axis = (gr-g) versus pre-test (x) of control class (T) and experiment class (ED)

To analyze differences of the two means of the experiment and control class, post-test scores used the Wilcoxon W Test as shown in Tables 3 and 4 which show significance of (0.000) - less than 0.05. This indicates that there are significant differences in mean post-test scores between the experimental class and traditional class. Based on the mean (average), the average grade post-test experimental scores are greater than the average post-test scores of a traditional class. The results indicate that the students' experimental design skills are better than the students' traditional class.

Table 3. Wilcoxon Signed Ranks Test

Ranks

		N	Mean Rank	Sum of Ranks
posttest_ED - pretest_ED	Negative Ranks	9[a]	5,67	51,00
	Positive Ranks	1[b]	4,00	4,00
	Ties	30[c]		
	Total	40		
posttest_T - pretest_T	Negative Ranks	40[d]	20,50	820,00
	Positive Ranks	0[e]	,00	,00
	Ties	0[f]		
	Total	40		

Table 4. Test Statistics[b]

	posttest_ED - pretest_ED	posttest_T - pretest_T
Z	-2,489[a]	-5,515[a]
Asymp. Sig. (2-tailed)	,013	,000

a. Based on positive ranks.

b. Wilcoxon Signed Ranks Test

The Joko Tingkir Program, when used as a Learning Tool for Tsunami Warning implementation, can improve experiment design skills for students, because it encourages them to demonstrate their ability with an expectation of an outcome. Students, who focus on investigating a tsunami phenomenon without having expectations of its outcomes, do not fare as well as the students who have such expectations based on established tsunami concepts or relationships – the latter being able to better address practical problems.

Furthermore, the use of the Joko Tingkir Program with FQS can encourage students to explore the possible variations of a research topic before attempting to state a problem, write a hypothesis, identify variables, constants and the needed control. Students need a method that is tried and used several times before using measures of tsunami parameters in designing an original experiment of their own. This finding is in good agreement with what is supported by the Cothron et al. (1989) reference.

A plot of average gain (gr) and individual gain (g) difference (gr-g) versus pre-test scores of the experiment class that using the Joko Tingkir Program with the FQS shows a strong positive correlation with regression (gr-g) = 0.1615 (pre-test scores) - 0.3336. A plot of average gain (gr) and individual gain (g) difference (gr-g) versus pre-test scores of the control class that uses traditional method (laboratory activity, using receipt laboratory and passive student), shows a positive correlation with regression (gr-g) = 0.0353 (pre-test scores) + 0.2402.

5. CONCLUSIONS

Based on the gain analysis it can be inferred that the experiment design skills can be improved by implementation of the Joko Tingkir Program as a Learning Tool for Tsunami Warning understanding.

ACKNOWLEDGMENTS

This work was supported by Unggulan Perguruan Tinggi (UNESA) Grants No.: 024.3/UN38.11-p/LT/2014, funded by the Islamic Development Bank (IDB). We thank Dr. George Pararas-Carayannis, of Tsunami Society International for editing sections of this paper to improve on clarity.

REFERENCES

Anderson-Cook CM, Dorai-Raj S (2001) An active learning in-class demonstration of good experimental design. J Stat Educ 9. http://www.amstat.org/publications/jse/v9n1/anderson-cook.html

Bao, L., (2006). Theoretical comparisons of average normalized gain calculations. Am. J. Phys., Vol. 74, No. 10, October 2006

Bilek, S. L. and Lay, T., 1999. Rigidity variations with depth along megathrust faults in subduction zones, NATURE, Vol. 400, 29 July 1999, www.nature.com

Cothron, J. H., Giese, R. N., & Rezba, R. J. (1989). Students and research: Practical strategies for science classrooms and competitions (2nded.). Dubuque, IA: Kendall/Hunt.

Etkina, E., Alan Van Heuvelen, Suzanne White-Brahmia, David T. Brookes, Michael Gentile, Sahana Murthy.

David Rosengrant, and Aaron Warren. 2006. Scientific abilities and their assessment. PHYSICAL REVIEW SPECIAL TOPICS - PHYSICS EDUCATION RESEARCH **2**, 020103.

Festing MFW (2003) Principles: the need for better experimental design. Trends Pharmacol Sci 24:341-345.

Geist, E. and Yoshioka, S., 1996. Source Parameters Controlling the Generation and Propagation of Potential Local Tsunamis, NaturalHazards 13: 151-177.

Geist, E. L. & Bilek, S. L., 2001. Effect of depth-dependent shear modulus on tsunami generation along subduction zones, Geophys. Res. Lett., 28, 1315–1318, doi:10.1029/2000GL012385.

Hiebert SM (2007) Teaching simple experimental design to undergraduates: do your students understand the basics? Adv Physiol Educ 31:82-92.

Karelina, A. and Etkina, E. (2007). Acting like a physicist: Student approach study to experimental design. PHYSICAL REVIEW SPECIAL TOPICS - PHYSICS EDUCATION RESEARCH **3**, 020106.

Kolen, M. J., Zeng, L., & Hanson, B. A. (1996). Conditional standard errors of measurement forscale scores using IRT. Journal of Educational Measurement, 33, 129-140.

Lay, T., Kanamori, H., Ammon, C. J., Nettles, M., Ward, S. N., Aster, R. C., Beck, S. L., Bilek, S. L., Brudzinski, M. R., Butler, R., DeShon, H. R., Ekstrom, G., Satake, K. and Sipkin, S., 2005. The great Sumatra- Andaman earthquake of 26 December 2004, Science, 308, 1127–1133.

Lomax, A. & Michelini, A., 2009a. Mwpd: a duration-amplitude procedure for rapid determination of earthquake magnitude and tsunamigenic potential from P waveforms, Geophys. J. Int., 176, 200–214, doi :10.1111/j.1365-246X.2008.03974.x.

Lomax, A. & Michelini, A., 2009b. Tsunami early warning using earthquake rupture duration, Geophys. Res. Lett., 36, L09306, doi :10.1029/2009GL037223.

Lomax, A. And A. Michelini, 2011. Tsunami early warning using earthquake rupture duration and P-wve dominant period: the importance of length and depth of faulting, Geophys. J. Int. 185, 283-291, doi: 10.1111/j.1365-246X.2010.04916.x.

Madlazim (2013), Assessment of Tsunami Generation Potential through Rapid Analysis of Seismic Parameters Case study: Comparison of the Earthquakes of 6 April and of 25 October 2010 of Sumatra, science of tsunami hazards 1 (32),

Madlazim (2012a), Toward tsunami early warning system in Indonesia by using rapid rupture durations estimation, AIP Conf. Proc. 1454, pp. 142-145; doi:http://dx.doi.org/10.1063/1.4730707 (4 pages) INTERNATIONAL CONFERENCE ON PHYSICS AND ITS APPLICATIONS: (ICPAP 2011).

Madlazim, 2011a. CMT, Fault Plane and Rupture Duration for Earthquakes in Sumatra and Possibility of its Implementation for Tsunami Early Warning System, PhD Program of Technology Sepuluh Nopember Institute (ITS) Surabaya. Dissertation.

Madlazim, 2011b. Toward Indonesian Tsunami Early Warning System by Using Rapid Rupture Durations Calculation, Science of tsunami hazards, 4(30).

Madlazim, Bagus Jaya Santosa, Jonathan M. Lees and Widya Utama, 2010. Earthquake Source Parameters at Sumatran Fault Zone: Identification of the Activated Fault Plane, Cent. Eur. J. Geosci. 2(4), 2010. DOI:10.2478/v10085-010-0016-5.

Masturyono, Madlazim, Thomas Hardy, and Karyono. In the 3rd International Symposium on Earthquake and Disaster Mitigation (ISEDM), Yogyakarta, 17-18 December 2013.

Okal, E.A., 1988. Seismic parameters controlling far-field tsunami amplitudes: a review, Nat. Hazards, 1, 67–96.

Pararas-Carayannis, G., 2013. "The Great Tohoku-Oki Earthquake and Tsunami of March 11, 2011 in Japan: A Critical Review and Evaluation of the Tsunami Source Mechanism," Pure and Applied Geophysics, pp. 1-22, 2013.

Polet, J. & Kanamori, H., 2009. Tsunami Earthquakes, in *Encyclopedia of Complexity and Systems Science,* p. 10370, ed.Meyers, A., Springer, New York, doi:10.1007/978-0-387-30440-3_567.

Satake, K., 1994. Mechanism of the 1992 Nicaragua tsunami earthquake, *Geophys. Res. Lett.,* **21**(23), 2519–2522

Satake, K., 2002. Tsunamis, in *International Handbook of Earthquake and Engineering Seismology,* pp. 437–451, eds Lee, W.H.K., Kanamori, H., Jennings, P.C. & Kisslinger, C., Academic Press, Amsterdam.

ISSN 8755-6839

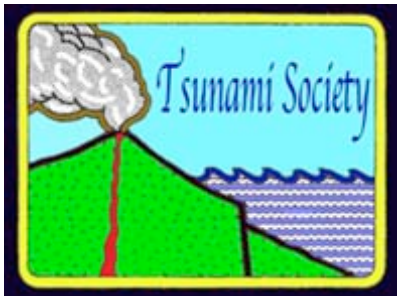

SCIENCE OF **TSUNAMI HAZARDS**

Journal of Tsunami Society International

Volume 33 **Number 2** **2014**

TSUNAMI SOCIETY INTERNATIONAL, 1741 Ala Moana Blvd. #70, Honolulu, HI 96815, USA.

WWW.TSUNAMISOCIETY.ORG